

## 1 **Germline genomic and phenomic landscape of clonal hematopoiesis in 323,112** 2 **individuals**

3 Md Mesbah Uddin<sup>\*1,2</sup>, Zhi Yu<sup>\*1,2</sup>, Joshua S. Weinstock<sup>3</sup>, Tetsushi Nakao<sup>1,2,4,5</sup>, Abhishek  
4 Niroula<sup>4,6,7</sup>, Sarah M. Urbut<sup>1,8</sup>, Satoshi Koyama<sup>1,2</sup>, Seyedeh M. Zekavat<sup>1,2,9</sup>, Kaavya Paruchuri<sup>1,2,10</sup>,  
5 Alexander J. Silver<sup>11</sup>, Taralynn M. Mack<sup>12</sup>, Megan Y. Wong<sup>1,2</sup>, Sara M. Haidermota<sup>1,2</sup>, Romit  
6 Bhattacharya<sup>1,2,8</sup>, Saman Doroodgar Jorshery<sup>13-15</sup>, Michael A. Raddatz<sup>11</sup>, Michael C.  
7 Honigberg<sup>1,2,8</sup>, Whitney E. Hornsby<sup>16</sup>, Martin JinYE Zhang<sup>13,17</sup>, Vijay G. Sankaran<sup>6,18-20</sup>, Gabriel  
8 K. Griffin<sup>21-23</sup>, Christopher J. Gibson<sup>4</sup>, Hailey A. Kresge<sup>11</sup>, Patrick T. Ellinor<sup>1,2</sup>, Veterans Affairs'  
9 Million Veteran Program<sup>24</sup>, Kelly Cho<sup>25,26</sup>, Yan V. Sun<sup>27,28</sup>, Peter W.F. Wilson<sup>27,29</sup>, Saiju  
10 Pyarajan<sup>25,26</sup>, Giulio Genovese<sup>13,30,31</sup>, Yaomin Xu<sup>32,33</sup>, Michael R. Savona<sup>11</sup>, Alexander P.  
11 Reiner<sup>34,35</sup>, Siddhartha Jaiswal<sup>36,37</sup>, Benjamin L. Ebert<sup>4,6,38</sup>, Alexander G. Bick<sup>#12</sup>, and Pradeep  
12 Natarajan<sup>#1,2,10</sup>

13

14 \*Contributed equally to this work

15 #Jointly supervised this work

16 Correspondence: [alexander.bick@vumc.org](mailto:alexander.bick@vumc.org) (A.G.B.) and [pnatarajan@mgh.harvard.edu](mailto:pnatarajan@mgh.harvard.edu) (P.N.)

17

- 18 1. Program in Medical and Population Genetics and Cardiovascular Disease Initiative, Broad  
19 Institute of Harvard and MIT, Cambridge, MA 02142, USA
- 20 2. Cardiovascular Research Center and Center for Genomic Medicine, Massachusetts  
21 General Hospital, Boston, MA 02114, USA
- 22 3. Department of Biostatistics, University of Michigan School of Public Health, Ann Arbor,  
23 MI, USA
- 24 4. Department of Medical Oncology, Dana-Farber Cancer Institute, Boston, MA 02115, USA
- 25 5. Division of Cardiovascular Medicine, Department of Medicine, Brigham and Women's  
26 Hospital, Boston, MA 02115, USA
- 27 6. Broad Institute of Harvard and MIT, Cambridge, MA 02142, USA
- 28 7. Department of Laboratory Medicine, Lund University, Lund, Sweden
- 29 8. Cardiology Division, Department of Medicine, Massachusetts General Hospital, Boston,  
30 MA 02114, USA
- 31 9. Computational Biology & Bioinformatics Program, Yale University, New Haven, CT,  
32 06510, USA
- 33 10. Department of Medicine, Harvard Medical School, Boston, MA, USA
- 34 11. Vanderbilt University School of Medicine, Nashville, TN, USA
- 35 12. Division of Genetic Medicine, Department of Medicine, Vanderbilt University Medical  
36 Center, Nashville, TN, USA
- 37 13. Program in Medical and Population Genetics, Broad Institute of MIT and Harvard,  
38 Cambridge, MA, USA

- 39 14. Department of Computer Science, University of Toronto, Toronto, Canada
- 40 15. Department of Computer Science and Electrical Engineering, Massachusetts Institute of
- 41 Technology, Cambridge, MA, USA
- 42 16. Center for Genomic Medicine, Massachusetts General Hospital, Boston, MA 02114, USA
- 43 17. Department of Epidemiology, Harvard T.H. Chan School of Public Health, Boston, MA,
- 44 USA
- 45 18. Division of Hematology/Oncology, Boston Children's Hospital, Harvard Medical School,
- 46 Boston, USA
- 47 19. Department of Pediatric Oncology, Dana-Farber Cancer Institute, Harvard Medical School,
- 48 Boston, USA
- 49 20. Harvard Stem Cell Institute, Cambridge, USA
- 50 21. Department of Pathology, Dana-Farber Cancer Institute, Boston, MA 02215, USA
- 51 22. Division of Hematopathology, Department of Pathology, Brigham and Women's Hospital,
- 52 Boston MA 02115, USA
- 53 23. Epigenomics Program, Broad Institute of MIT and Harvard, Cambridge, MA, USA
- 54 24. A full list of authors appears in the Supplementary Note
- 55 25. Veterans Affairs Boston Healthcare System, Boston, MA, USA
- 56 26. Department of Medicine, Brigham and Women's Hospital, Harvard Medical School,
- 57 Boston, MA, USA
- 58 27. Veterans Affairs Atlanta Healthcare Systems, Decatur, Georgia, USA
- 59 28. Department of Epidemiology, Emory University Rollins School of Public Health, Atlanta,
- 60 Georgia, USA
- 61 29. Department of Medicine, Emory University School of Medicine, Atlanta, Georgia, USA
- 62 30. Stanley Center for Psychiatric Research, Broad Institute of MIT and Harvard, Cambridge,
- 63 MA 02142, USA
- 64 31. Department of Genetics, Harvard Medical School, Boston, MA 02115, USA
- 65 32. Department of Biostatistics, Vanderbilt University Medical Center, Nashville, Tennessee,
- 66 USA
- 67 33. Department of Biomedical Informatics, Vanderbilt University Medical Center, Nashville,
- 68 Tennessee, USA
- 69 34. Public Health Sciences Division, Fred Hutchinson Cancer Center, Seattle WA 98109, USA
- 70 35. Department of Epidemiology, University of Washington, Seattle WA 98195, USA
- 71 36. Department of Pathology, Stanford University School of Medicine, Stanford, CA, USA
- 72 37. Institute for Stem Cell Biology and Regenerative Medicine, Stanford University School of
- 73 Medicine, Stanford, CA, USA
- 74 38. Howard Hughes Medical Institute, Boston, MA, USA

75 **Abstract**

76 With age, acquired mutations can cause clonal expansion of hematopoietic stem cells (HSC). This  
77 clonal hematopoiesis of indeterminate potential (CHIP) leads to an increased predisposition to  
78 numerous diseases including blood cancer and cardiovascular disease. Here, we report multi-  
79 ancestry genome-wide association meta-analyses of CHIP among 323,112 individuals (19.5%  
80 non-European; 5.3% have CHIP). We identify 15 genome-wide significant regions and nominate  
81 additional loci through multi-trait analyses, and highlight variants in genes involved in self-  
82 renewal and proliferation of HSC, telomere maintenance, and DNA damage response pathways.  
83 We then use Mendelian randomization to establish a causal relationship between CHIP and  
84 coronary artery disease. Next, we systematically profile consequences of CHIP across the  
85 phenome, which revealed strong associations with hematopoietic, neoplastic, and circulatory  
86 conditions corroborated by polygenic enrichment of CHIP loci in immune cells and  
87 cardiomyocytes. These findings expand the genomic and phenomic landscape of CHIP.

88

## 89 Introduction

90 Self-renewing cell populations accumulate somatic mutations with aging, although most  
91 of these mutations are without functional consequence. In rare cases, these somatic mutations  
92 confer a selective advantage leading to clonal expansion<sup>1-3</sup>. In the case of hematopoietic stem cells,  
93 driver mutations in genes with diverse functions, including DNA methylation (*DNMT3A*, *TET2*)<sup>4,5</sup>,  
94 RNA splicing (*SF3B1*, *U2AF1*)<sup>6</sup>, chromatin remodeling (*ASXL1*)<sup>7</sup>, and DNA damage response  
95 (*TP53*, *PPM1D*)<sup>8-10</sup> can lead to a clonal expansion of hematopoietic stem cells termed clonal  
96 hematopoiesis of indeterminate potential (CHIP) when such mutations make up >4% of peripheral  
97 blood cells (variant allele fraction, VAF $\geq$ 2%). CHIP is the pre-cancerous precursor lesion for  
98 myeloid hematologic malignancy<sup>11-13</sup>, but numerous studies in human and model systems have  
99 linked CHIP to diverse diseases of aging, including coronary artery disease<sup>14,15</sup>, stroke<sup>16</sup>, heart  
100 failure<sup>17</sup>, chronic obstructive pulmonary disease<sup>18</sup>, osteoporosis<sup>19</sup>, and chronic liver disease<sup>20</sup>.  
101 However, CHIP is less commonly observed among patients with Alzheimer's disease<sup>21</sup>.  
102 Characterizing the germline genetic determinants of CHIP offers the opportunity to prioritize  
103 unifying features of multiple diseases of aging.

104 We previously performed a genome-wide association study (GWAS) of CHIP and  
105 identified three genomic regions associated with CHIP risk in a study of 3,831 CHIP cases and  
106 61,574 controls from whole-genome sequencing of blood DNA utilizing the National Heart, Lung  
107 and Blood Institute (NHLBI) Trans-Omics for Precision Medicine (TOPMed) study<sup>22</sup>. This effort  
108 identified three germline genetic variants, including one in the *TERT* promoter, the intronic region  
109 of *TRIM59*, and a distal enhancer of *TET2* specific to individuals of African ancestry. These  
110 findings enabled further work demonstrating that the low-frequency germline variant at *TET2*  
111 leads to locally altered methylation and decreased germline *TET2* expression, subsequently  
112 promoting the self-renewal and proliferation of hematopoietic stem cells<sup>22</sup>. Furthermore,  
113 bidirectional Mendelian randomization analyses of leukocyte telomere length (LTL), *TERT* locus  
114 variants, and CHIP highlight the dynamic nature of genomic models across the lifespan<sup>23</sup>.

115 Here, we analyze 17,044 CHIP cases and 306,068 controls across four cohorts, including  
116 63,442 (19.5%) individuals of non-European ancestry from whole-genome or whole-exome  
117 sequencing of blood DNA. Using this expanded dataset, we perform genome-wide discovery  
118 analyses and fine-mapping at both variant<sup>24</sup> and gene levels<sup>25</sup>. We identify multiple components  
119 of the DNA damage response pathways<sup>26,27</sup> that lead to CHIP, unifying epidemiological  
120 observations regarding enhanced CHIP risk in populations with specific environmental or  
121 cytotoxic exposures<sup>8,28,29</sup>. Multivariate Bayesian analyses with myeloproliferative neoplasm  
122 (MPN)-associated alleles<sup>30</sup> further prioritize several additional loci. Finally, we leverage this  
123 expanded dataset to systematically profile the disease risk of CHIP compared to another form of  
124 clonal hematopoiesis—mosaic chromosomal alterations (mCAs), and further investigate the  
125 disease associations by examining cell types<sup>31</sup> enriched by CHIP (**Extended Data Fig. 1**).

## 126 Results

### 127 Baseline characteristics

128 We analyzed 355,183 individuals across four cohorts, UK Biobank (UKB; N=200,128),  
129 TOPMed (N=87,116), Vanderbilt BioVU (N=54,583), and Mass General Brigham Biobank  
130 (MGBB; N=13,356) for CHIP mutations using previously described methods (see **Methods**).  
131 These individuals are of European (N=287,991), African (N=31,900), Asian (N=14,073), Hispanic  
132 (N=13,939), and other or unknown (N=7,280) ancestry (**Supplementary Table 1**). We identified  
133 20,302 CHIP mutations in 18,499 individuals (5.2%). Consistent with previous reports<sup>22</sup>, CHIP  
134 was robustly associated with age (**Fig. 1a**) and had a similar distribution of genes identified in  
135 prior studies. Across all cohorts, 90.8% of individuals with CHIP driver mutations had only one  
136 identified mutation (**Fig. 1b**). *DNMT3A*, *TET2*, and *ASXL1* are the most frequent mutated genes,  
137 accounting for more than 75% of CHIP mutations (**Fig. 1c**). Compared with other cohorts, MGBB  
138 has a relatively lower proportion of individuals with *DNMT3A* mutations but a relatively larger  
139 proportion with *TET2* mutations. The next seven most frequent genes are *PPM1D*, *TP53*, *JAK2*,  
140 *SF3B1*, *SRSF2*, *GNB1*, and *CBL*. For most of these top mutated genes, the corresponding VAF for  
141 participants in TOPMed are larger than that seen in other cohorts, which is likely explained by  
142 technical sensitivities between whole-genome (TOPMed) and whole-exome (UKB and MGBB)  
143 sequencing-based CHIP detection. The median VAF of *DNMT3A* was 0.08 in UKB, 0.13 in  
144 TOPMed, and 0.09 in MGBB; the median VAF of *TET2* was 0.11 in UKB, 0.16 in TOPMed, and  
145 0.09 in MGBB. *JAK2* has the largest clonal fraction among the top ten genes, with a median VAF  
146 of 0.30 in UKB, 0.21 in TOPMed, and 0.32 in MGBB (**Fig. 1d**). In BioVU, CHIP was identified  
147 in four driver genes, *DNMT3A*, *JAK2*, *TET2*, and *ASXL1*, using a customized genotyping array  
148 (see **Methods**). The most common mutations in BioVU samples were *JAK2* V617F and *DNMT3A*  
149 R882C/H.

### 150 Fifteen genome-wide significant loci associated with CHIP categories

151 We performed multi-ancestry meta-analyses of overall CHIP (pooled sample size, 17,044  
152 cases, and 306,068 controls), *DNMT3A* (8,949 cases and 307,971 controls), and *TET2* (2,851 cases  
153 and 307,527 controls) CHIP GWAS from TOPMed, UKB, MGBB, and BioVU. Here, we  
154 performed three GWAS for each of the four participating cohorts, followed by multi-ancestry  
155 meta-analyses using the fixed-effects inverse-variance-weighted approach (see **Methods**). A total  
156 of 323,112 participants and 21,455,227 variants (minor allele frequency (MAF) $\geq$ 0.1%; variants  
157 present in  $\geq$ two studies) remained after variant filtering and quality-control procedures. There  
158 was no evidence of artificial inflation of association statistics due to the population structure  
159 (genomic control factor  $\lambda_{GC}$  = 1.05 for CHIP and *DNMT3A*, 1.06 for *TET2*; **Fig. 2a-c**). The SNP  
160 heritability ( $h^2_{SNP}$ ) of overall CHIP among the entire study population was estimated at 3.5%  
161 (SD=0.002) on the observed scale and 15.8% (SD=0.011) on the liability scale using the BLD-  
162 LDAK model (see **Methods** and **Supplementary Table 2**), representing a four-fold increase from  
163 the previous estimate<sup>22</sup>.

164 We discovered ten loci associated with overall CHIP at genome-wide significance after  
165 correcting for multiple testing ( $P < 1.67 \times 10^{-8}$ , i.e.,  $5.0 \times 10^{-8}/3$ ). Seven of the loci are new and  
166 mapped to the following genes based on proximity of the lead variants: *PARP1*, *CDI64/SMPD2*,  
167 *ATM*, *ITPR2*, *MSI2*, *SETBP1*, and *CHEK2* (**Fig. 2a** and **Supplementary Tables 3,4**). Consistent  
168 with previous report<sup>22</sup>, the strongest signal remained at the *TERT* locus, with rs7705526-A as the  
169 lead variant (odds ratio (OR) (95% confidence interval (CI)) = 1.26 (1.23-1.29);  $P = 2.6 \times 10^{-81}$ ).  
170 Regional association plots are shown in **Extended Data Fig. 2**. The effects of associated SNPs  
171 were largely homogeneous across studies (i.e., heterogeneity  $P > 0.05$ , **Supplementary Tables**  
172 **3,4**). Summary-statistics-based conditional analysis yielded 12 independent SNPs that reached  
173 genome-wide significance at  $P < 1.67 \times 10^{-8}$  (**Supplementary Table 5**).

174 CHIP driver gene-specific association analyses identified ten loci associated with  
175 *DNMT3A* and six loci associated with *TET2* (**Fig. 2bc**, **Extended Data Fig. 3,4**, **Supplementary**  
176 **Tables 4, 6-9**). *TCLIA* is a newly discovered locus that significantly increased the risk for  
177 *DNMT3A* CHIP (rs2887399-T; OR (95% CI) = 1.19 (1.15-1.23);  $P = 1.26 \times 10^{-22}$ ) and significantly  
178 reduced the risk for *TET2* CHIP (rs4900291-T; OR (95% CI) = 0.78 (0.73-0.84);  $P = 2.92 \times 10^{-11}$ ).

179 Interestingly, there was a larger overlap of loci associated with overall CHIP and *DNMT3A*  
180 CHIP: nine of the ten loci were common between the two CHIP categories (**Fig. 2d**). CHIP-  
181 associated loci ( $P < 1.67 \times 10^{-8}$ ) also overlapped with LTL<sup>32</sup>, expanded mCAs<sup>33</sup>, and MPN<sup>30</sup>  
182 associated genome-wide significant loci ( $P < 5 \times 10^{-8}$ ). Here, seven, five, and three of the CHIP-  
183 associated loci overlapped with LTL, expanded mCAs, and MPN-associated loci, respectively  
184 (**Fig. 2d**).

185 We also conducted a joint multivariate analysis across MPN<sup>30</sup>, overall CHIP, *DNMT3A*,  
186 and *TET2* using empirical Bayes hierarchical modeling<sup>34</sup> (see **Methods**). This approach yielded a  
187 3-fold boost in power for discovery. Compared with conventional GWAS, we identified 39, 39,  
188 and 46 more genetic regions for overall CHIP, *DNMT3A*, and *TET2* CHIP, respectively, with  
189 evidence for the association through this method (**Extended Data Fig. 5**).

## 190 **Statistical fine-mapping identified causal variants at *ATM* and *PARP1***

191 Statistical fine-mapping was conducted using the results of the European meta-analysis and  
192 LD matrix derived from the UKB European population to identify the causal variants in the  
193 associated loci (see **Methods**). We identified 27 variants with posterior inclusion probability (PIP) >  
194 10% (**Supplementary Table 10**), among which a missense variant, rs1800057-G, in the newly  
195 discovered *ATM* gene (ENST00000675843.1:c.3161C>G;p.Pro1054Arg; OR (95% CI) = 1.28  
196 (1.18-1.37);  $P = 1.3 \times 10^{-10}$ ) showed higher posterior probability of inclusion (PIP 22%) in the locus  
197 (**Fig. 3a**). The risk allele for this coding variant was predicted to be deleterious by various  
198 functional annotation tools (**Fig. 3b**). Decreased function of the *ATM* gene and increased risk for  
199 CHIP aligns with the prior observation that the loss of function and low expression of *ATM* were  
200 associated with tumorigenesis and worse prognosis in various cancers, including MPN<sup>35,36</sup>. In  
201 another newly discovered locus at *PARP1*, we identified a non-coding variant, rs1527365-T, with

202 high posterior probability (PIP=33%; OR (95% CI) = 0.88 (0.85-0.91);  $P=7.0 \times 10^{-13}$ ), which is  
203 the lead variant in European meta-analysis of CHIP GWAS (**Fig. 3c**). The T allele at rs1527365 is  
204 protective for overall CHIP and *DNMT3A* CHIP (**Supplementary Tables 3,6**) and associated with  
205 decreased expression of *PARP1* in whole blood (**Fig. 3d**; normalized effect size=-0.067,  
206  $P=1.7 \times 10^{-4}$ , GTEx v8). This is consistent with the observations that a higher expression of *PARP1*  
207 is a marker for worse clinical outcomes in various tumors, including myeloid leukemia, and that  
208 inhibition of *PARP1* has anti-tumor effects<sup>37</sup>. rs1527365 is also a cis-methylation QTL where the  
209 T allele is associated with increased DNA methylation at CpGs around *PARP1* (data from  
210 GoDMC<sup>38</sup>:<http://mqtlldb.godmc.org.uk/>), further supporting the negative regulation of *PARP1* by  
211 this allele.

## 212 **Similarity-based gene prioritization identified several putative causal genes**

213 Next, to prioritize causal genes from the GWAS data, we incorporated a novel gene  
214 prioritization method, Polygenic Priority Score (PoPS)<sup>25</sup>. PoPS combines GWAS data with other  
215 omics data (e.g., gene expression, biological pathway, and predicted protein-protein interaction)  
216 to prioritize casual genes based on functional similarity. We applied PoPS to summary-level data  
217 from the UKB GWAS results of overall CHIP, *DNMT3A*, and *TET2* using European ancestry  
218 individuals from the UKB study population as a reference panel. Features from gene expression  
219 data, protein-protein interaction networks, and pathway membership that passed a marginal feature  
220 selection step were included in the final predictive model (see **Methods**). We identified 26  
221 prioritized gene-trait pairs. Top putative causal genes prioritized by PoPS (PoPS score>0.3)  
222 included *PARP1*, *ITF80*, *TET2*, *TERT*, *SMPD2*, *ATM*, *ITPR2*, *MSI2*, and *CHEK2* for overall CHIP  
223 (**Supplementary Table 11**), *PARP1*, *ITF80*, *TERT*, *SMPD2*, *ATM*, *ITPR2*, *TCL1A*, *SETBP1*, and  
224 *CHEK2* for *DNMT3A* CHIP (**Supplementary Table 12**), and *AGTRAP*, *BDKRB2*, and *ZFPMI*  
225 for *TET2* CHIP (**Supplementary Table 13**). This prioritization corroborates with the fine-mapped  
226 causal variants at *PARP1*, *TERT*, and *ATM* as well as previously validated causal variants at  
227 *TET2*<sup>22</sup> and *TCL1A*<sup>39</sup>. Further, the consistency between prioritized genes by PoPS (similarity-  
228 based approach) and distance (non-similarity-based approach) suggest high confidence<sup>25</sup>.

## 229 **Mendelian randomization refined causality between CHIP and coronary artery 230 disease**

231 Leveraging the large CHIP meta-analysis, we used Mendelian randomization (MR) to  
232 understand the causality of CHIP and disease outcomes. Since CHIP has been associated with  
233 coronary artery disease (CAD) incidence in humans and atherosclerosis in a *Tet2* CHIP mouse  
234 model<sup>14,40,41</sup>, we performed MR analyses of overall CHIP, *DNMT3A*, and *TET2* with CAD. While  
235 genetic predispositions for CHIP overlapped with those for LTL, previous MR studies support  
236 inverse causality for LTL on CAD, implying complex causal relationships between CHIP-LTL,  
237 and LTL-CAD<sup>23</sup>. Thus, we carefully selected instrumental variables (IVs) to avoid clear violations  
238 of MR assumptions by excluding IVs 1) associated with known confounders between CHIP and  
239 CAD, including hypercholesterolemia, hypertension, type 2 diabetes, body mass index, smoking

240 status, or 2) having more robust associations with LTL than with CAD, and/or 3) having inverse  
241 effect sizes for LTL, CHIP, and CAD, accounting for the inverse causal association between LTL  
242 and CAD. Mendelian randomization using the robust adjusted profile score (MR-RAPS) was used  
243 given the limited power for CHIP analyses due to low heritability, especially the gene-specific  
244 analyses. MR-RAPS is a novel method that accommodates weak instruments in the MR framework.  
245 The approach was used as our primary method, and a liberal p-value threshold was applied for IV  
246 selections (see **Methods**)<sup>42</sup>. Using summary statistics of multi-ancestry meta-analysis for CHIP,  
247 we observed significant positive causal effects of genetically-determined *TET2* CHIP mutation  
248 risk on CAD risk ( $P=3.2 \times 10^{-4}$ ). In contrast, the overall CHIP and *DNMT3A* CHIP mutation results  
249 were null, consistent with differential causal effects on CAD risk by CHIP mutated gene types  
250 (**Fig. 4**). However, sensitivity analyses using other MR approaches that do not allow for weak  
251 instruments yielded null results across overall CHIP, *DNMT3A*, and *TET2* CHIP mutations  
252 (**Extended Data Fig. 6 and Supplemental Tables 14-16**).

### 253 **Phenome-wide scans yielded different patterns between CHIP and mCAs**

254 The dataset assembled now permits a comprehensive and well-powered phenome-wide  
255 association study (PheWAS) of CHIP. At the same time, we contrast CHIP with a different age-  
256 associated clonal hematopoietic phenomenon, mosaic chromosomal alterations (mCAs) (see  
257 **Methods**). We not only compared the CHIP and mCAs in the same study population where  
258 information on both is available, but we also examined the mCAs in an extended dataset (N=  
259 1,116,579) as a secondary analysis to maximize the discovery power.

260 Among incident hematopoietic and neoplastic conditions (**Fig. 5a and Supplementary**  
261 **Table 17**), significant associations were observed with leukemias [CHIP: hazard ratio (HR)  
262 =1.78, 95% CI 1.42 - 2.24, FDR= $1.76 \times 10^{-4}$ ; autosomal mCAs: HR=6.87, FDR= $5.81 \times 10^{-89}$ ],  
263 with the largest effect for expanded CHIP (i.e., VAF>10%) and myeloid leukemias (HR 11.56,  
264 95% CI 6.67 - 20.06, FDR= $3.67 \times 10^{-15}$ ) and for expanded autosomal mCAs and lymphoid  
265 leukemias (HR 78.36, 95% CI 57.55 - 106.69, FDR= $5.91 \times 10^{-166}$ ), as shown previously<sup>2,43</sup>.  
266 Besides hematopoietic malignancies, neoplastic associations were also detected with incident  
267 respiratory cancer (Expanded CHIP: HR 1.52, 95% CI 1.27 - 1.81, FDR= $4.05 \times 10^{-4}$ ), malignancies  
268 of the brain for CHIP (HR=1.84, 95% CI 1.31 - 2.58, FDR=0.025), and skin cancer for mCAs  
269 (Expanded autosomal mCAs: HR 1.45, 95% CI 1.15 - 1.82, FDR=0.024).

270 For CHIP, across other non-hematopoietic/neoplastic conditions, significant associations  
271 were observed with circulatory, gastrointestinal, genitourinary, renal, and infectious conditions,  
272 some of which showed consistent associations with mCAs (**Fig. 5b and Supplementary Table**  
273 **17**). In particular, among circulatory conditions, association with incident arterial embolism and  
274 thrombosis was detected for expanded *TET2* (HR=2.97, 95% CI 1.58 - 5.59, FDR=0.03). While  
275 no significant association for mCAs was detected among the same sample set analyzed for CHIP,  
276 a significant association with incident arterial embolism and thrombosis was detected for expanded  
277 mCAs (HR=1.17, 95% CI 1.08 - 1.27, FDR=0.0017) (**Supplementary Table 18 and Extended**



278 **Data Fig. 7**), particularly for expanded ChrX mCAs in females (HR=3.92, 95% CI 1.92 - 8.02,  
279 FDR=0.029). Additionally, significant associations with cardiomyopathy for CHIP (HR 1.64, 95%  
280 CI 1.30 - 2.07, FDR=0.0026) but not for mCAs were observed (**Supplementary Table 18 and**  
281 **Extended Data Fig. 7**). The following were other notable CHIP-specific cardiovascular  
282 associations: hypertension, pulmonary heart disease, and lower extremity varicose veins. While  
283 CHIP was not strongly associated with CAD in the PheWAS analysis, using solely combined ICD-  
284 9 and ICD-10 codes per the 'phecode' algorithm, further analyses using a more comprehensive  
285 CAD phenotype (composite of myocardial infarction, coronary revascularization, stroke, and death)  
286 yielded significant associations between CHIP and incident CAD (**Supplementary Table 19**).

287 Other than circulatory conditions (**Fig. 5b and Supplementary Table 18**), several  
288 additional incident phenotypic associations were observed. CHIP-specific associations included  
289 peptic ulcer disease and diverticulosis. mCAs and CHIP were similarly associated with acute renal  
290 failure and pneumonia, and mCAs had a larger association with splenomegaly. Additionally,  
291 mCAs were more strongly associated with sepsis and viral infections, while CHIP was more  
292 strongly associated with bacterial infections.

### 293 **Polygenic associations of CHIP at a single-cell level corroborated PheWAS findings**

294 We used scDRS<sup>31</sup> to assess the polygenic enrichment of the overall CHIP, *DNMT3A*, and  
295 *TET2* GWASs in different cell populations in 2 single-cell RNA sequencing (scRNA-seq) data  
296 sets, namely the Tabula Muris Senis (TMS) mouse cell atlas<sup>44</sup> and Tabula Sapiens (TS) human  
297 cell atlas<sup>45</sup>. scDRS assesses excess expression of GWAS-associated genes in single-cell data; we  
298 considered FDR<0.3 for significant association and P<0.01 for suggestive association (see  
299 **Methods**). Results are reported in **Figure 6**. We determined the polygenic signal in the CHIP  
300 GWAS is significantly more highly expressed in ventricular myocytes and atrial myocytes from  
301 the heart ( $P<0.001$ , and  $P=0.004$ , respectively) and neuronal stem cells and oligodendrocytes from  
302 the brain non-myeloid tissue ( $P=0.004$ , and 0.01 respectively). *DNMT3A* is suggestively more  
303 highly expressed in ventricular myocytes from the heart ( $P=0.003$ ). *TET2* is significantly more  
304 highly expressed in DN4 thymocytes from the thymus ( $P=0.002$ ) and suggestively in T cells  
305 ( $P=0.007$ ; combined from trachea, heart, brown adipose tissue, and limb muscle). Notably, the  
306 polygenic enrichment findings corroborate our PheWAS results and the existing literature<sup>14,21</sup>. The  
307 results are also consistent between TMS and TS (**Extended Data Fig. 8a**) and between cell type-  
308 level and tissue-level associations (**Extended Data Fig. 8b,c**). In addition, we assessed the  
309 robustness of the results by subsampling the TMS data and subsampling the putative trait gene  
310 sets. We determined that the results are consistent across the subsampling experiments (**Extended**  
311 **Data Figure 9**).

312

## 313 Discussion

314 In this large and diverse genetic study of CHIP, we identified ten genome-wide significant  
315 regions, including seven that are new and one that is driver gene-specific. We highlight variants in  
316 *ATM* and *PARP1* as causal CHIP variants leading to decreased DNA damage repair and a number  
317 of putative causal genes. We systematically profiled CHIP consequences phenome-wide and  
318 highlighted strong associations with hematopoietic, neoplastic, and circulatory conditions  
319 corroborated by the polygenic enrichments of CHIP in immune cells and myocytes. These findings  
320 provide an expanded genomic and phenomic landscape for clonal hematopoiesis.

321 Our study has several important findings. First, the relatively large sample size enabled  
322 better-powered delineations of potential mechanisms that contribute to CHIP and specific driver  
323 genes, including failure to repair DNA damage and differential clonal competitive advantage.  
324 Among the newly discovered CHIP-associated genes, *ATM* has been significantly associated with  
325 the *JAK2 V617F* clonal hematopoiesis and MPNs<sup>46</sup>, and it is a core component of the DNA repair  
326 system, and the fine-mapped missense variant on this gene is predicted to decrease its function<sup>47</sup>.  
327 Also, high *PARP1* expression has been shown to exacerbate DNA damage<sup>48</sup>, and the fine-mapped  
328 regulatory variant, which reduces CHIP risk, decreases *PARP1* expression in the human blood  
329 cells. Driver gene-specific GWAS showed differential association patterns for *DNMT3A* and *TET2*  
330 CHIP mutations. In particular, we observed significant signals at the *TCL1A* locus for both  
331 *DNMT3A* and *TET2*, with the direction of effects being opposite. *TCL1A* has been observed to  
332 implicate in B-cell and T-cell and malignancies<sup>49,50</sup>, and its encoded protein is thought to promote  
333 Akt activity, which is central to many signaling pathways, such as cellular proliferation, growth,  
334 and survival<sup>51,52</sup>. Recent evidence using gene expression data suggested activation of *TCL1A* as an  
335 event driving clonal expansion for *TET2*, but not for *DNMT3A*<sup>39</sup> and our GWAS findings provide  
336 further evidence to support that finding. These findings indicate that while driver mutations  
337 ultimately yield CHIP, their respective heritable bases have shared and distinct heritable factors.

338 Second, we found that the specific somatic mutation in the hematopoietic stem cell clone  
339 was indicative of specific disease consequences. We conducted a phenome-wide scan for overall  
340 CHIP and individual driver mutations and contrasted CHIP with a distinct clonal hematopoietic  
341 phenomenon, lymphoid-biased mCAs. We observed associations of CHIP and mCAs with clonal  
342 hematopoiesis, hematologic malignancy, and non-malignant diseases linked to aging, with  
343 leukemia showing the strongest association followed by circulatory, gastrointestinal, genitourinary,  
344 renal, and infectious conditions, most of which showed consistent associations between CHIP and  
345 mCAs. However, marked heterogeneity was also observed between CHIP and mCAs. For example,  
346 unique protective associations for ChrY mCAs and cardiomyopathy in males were observed, while  
347 opposing effects between CHIP and mCAs on essential hypertension, pulmonary heart disease,  
348 and lower extremity varicose veins were observed.

349 Third, the application of novel statistical methods yielded new insights into CHIP biology.  
350 In alignment with the differential pheWAS associations between *DNMT3A* and *TET2* CHIP  
351 mutations, our MR analyses demonstrated their differential causal effects on CAD. We observed

352 a significant causal effect of genetically determined increased risk for acquiring *TET2* CHIP  
353 mutation on an increased risk for CAD, whereas the causal relationship was null for *DNMT3A*.  
354 Furthermore, our study leveraged a novel statistical approach to access the polygenic enrichment  
355 of CHIP, *DNMT3A*, and *TET2* in scRNA-seq data<sup>31</sup>. Corroborating the significant cardiomyopathy  
356 association in pheWAS results, CHIP had the strongest involvement with ventricular myocytes  
357 and atrial myocytes, while *DNMT3A* and *TET2* demonstrated different suggestive association  
358 patterns at the cell-type level. Lastly, using an empirical Bayes hierarchical approach for jointly  
359 modeling multiple traits<sup>34</sup>, we leveraged the high correlation between MPN and CHIP variables  
360 and nominated three-fold additional genetic regions that contain strong signals for CHIP,  
361 *DNMT3A*, and *TET2*.

362 Important limitations of our study include that many of the newly analyzed samples are of  
363 European ancestry, limiting our ability to benefit from the full diversity of genetic variation present  
364 in diverse ancestries. Second, the cross-sectional nature of our CHIP analysis limits conclusions  
365 regarding the temporal evolution between CHIP and these diseases. Third, the technical sensitivity  
366 of whole genome and whole exome sequencing precludes the ability to evaluate the clinical  
367 significance of CHIP mutations at low VAF.

368 Overall, our analyses of the inherited basis of CHIP identified new mechanisms affecting  
369 somatic mutation acquisition and clonal fitness with an expanded appreciation for how these  
370 somatic mutations shape disease phenotypes.

371

## 372 **Methods**

### 373 **Study population**

374 UK Biobank (UKB) is a prospective cohort study of ~500,000 participants (age range 40-  
375 69 at enrollment) from across the United Kingdom with deep genetic (DNA isolated from blood)  
376 and phenotypic data<sup>53</sup>. The present study was conducted under UKB application ID 7089 and  
377 50834. Secondary use of these data was approved by the Mass General Brigham Institutional  
378 Review Board (protocol 2021P002228).

379 TOPMed is a research program generating genomic data from DNA isolated from blood  
380 and other -omics data for more than 80 NHLBI-funded research studies with extensive phenotype  
381 data<sup>22,54</sup>. A total of 51 studies with diverse reported ethnicity (40% European, 32% African, 16%  
382 Hispanic/Latino, 10% Asian) were included in the Freeze 6 ([https://topmed.nhlbi.nih.gov/topmed-  
383 whole-genome-sequencing-methods-freeze-6](https://topmed.nhlbi.nih.gov/topmed-whole-genome-sequencing-methods-freeze-6)). Each of the included studies provided informed  
384 consent. Secondary analysis of the TOPMed data was approved by the Mass General Brigham  
385 Institutional Review Board (protocol 2016P001308). All relevant ethics committees approved this  
386 study, and this work is compliant with all applicable ethical regulations.

387 Mass General Brigham Biobank (MGBB)<sup>55</sup> is a volunteer biobank of patients receiving  
388 care at Mass General Brigham with electronic health records and genetic and phenotypic data on  
389 ~50,000 participants (<https://biobank.massgeneralbrigham.org/>). The present secondary analyses  
390 were approved by the Massachusetts General Hospital Institutional Review Board (protocol  
391 2018P001236).

392 BioVU, the Vanderbilt DNA Databank, is a de-identified biorepository that includes DNA  
393 from the peripheral blood remaining from routine clinical testing of approximately 250,000  
394 patients<sup>56,57</sup>. The present secondary analyses were approved by the Vanderbilt University Medical  
395 Center Institutional Review Board (IRB #201783).

396

397

## 398 **CHIP detection**

### 399 ***UKB***

400 Whole exome sequencing of whole blood DNA of 200,628 participants was used to identify  
401 somatic mutations. We selected 500 random youngest samples for panel-of-normal (PON) and  
402 called somatic mutations on the remaining 200,128 samples using Mutect2 software<sup>58</sup> in the Terra  
403 platform (<https://portal.firecloud.org/?return=terra#methods/gatk/mutect2-gatk4/20>). PON was  
404 used to minimize sequencing artifacts, and Genome Aggregation Database (gnomAD)<sup>59</sup> was used  
405 to filter likely germline variants from the putative somatic mutations call set. Each Variant Call  
406 Format (VCF) file was annotated using ANNOVAR software<sup>60</sup>, and putative CHIP mutations were  
407 identified using the pipeline described in Bick et al.<sup>22</sup> (<https://app.terra.bio/#workspaces/terra-outrreach/CHIP-Detection-Mutect2>; last accessed Feb 7, 2022). For identifying CHIP, pathogenic  
408 variants were queried in 74 genes known to drive clonal hematopoiesis and myeloid malignancies  
409 (list of variants queried is presented in **Supplementary Table 20**)<sup>22</sup>. We kept variants for further  
410 curation if (i) total depth of coverage  $\geq 10$ , (ii) number of reads supporting the alternate allele  $\geq 3$ ,  
411 (iii)  $\geq 1$  read in both forward and reverse direction supporting the alternate allele, and (iv)  
412 VAF  $\geq 0.02$ . Finally, CHIP mutations that passed sequence-based filtering were manually curated  
413 by a team of hematopathologists. The median depth of coverage was 77 (mean=80; SD=31.2;  
414 range 9-305), and the median number of supporting reads were 7 (mean=10; SD=8.6; range 3-101)  
415 in the final CHIP call set.  
416

417

### 418 ***NHLBI TOPMed***

419 Whole-genome sequencing of blood DNA was performed on 97,691 samples from Freeze 8  
420 NHLBI TOPMed data with a mean depth of at least 30 $\times$  using Illumina HiSeq X Ten instruments.  
421 All sequences in CRAM files were remapped to the hs38DH 1000 Genomes build 38 human  
422 genome reference, following the protocol published previously<sup>61</sup>. Single nucleotide

423 polymorphisms (SNP) and short indels were jointly discovered and genotyped across the TOPMed  
424 samples using the GotCloud pipeline<sup>62</sup>. The procedure used for CHIP and germline variants calling  
425 has been previously described<sup>22,63</sup>.

#### 426 ***MGBB***

427 Whole exome sequencing with an average coverage of 55× from whole blood DNA samples was  
428 performed for 13,356 MGBB participants. The procedure used for UKB CHIP calling (described  
429 above) was also applied for whole exome sequencing data in MGBB. Here, PON was created from  
430 100 random whole exome sequencing samples from the youngest participants (age at enrolment  
431  $\leq 21$ y). Putative CHIP mutations that passed the minimum depth of coverage ( $\geq 20$ ) and supporting  
432 reads threshold were manually curated to arrive at the final CHIP call set.

433

#### 434 ***Vanderbilt BioVU***

435 Among 54,583 participants of the Vanderbilt BioVU, CHIP was identified in DNA genotyped on  
436 the Illumina Multi-Ethnic Genotyping Array-Expanded (MEGA<sup>EX</sup>) for somatic mutations in four  
437 known CHIP driver genes: *DNMT3A*, *JAK2*, *TET2*, and *ASXL1*. We examined nonsense, splice  
438 site, and previously reported missense variants that are genotyped on the MEGA<sup>EX</sup> array, totaling  
439 29 CHIP mutations. B-allele fractions (BAF) were calculated from the intensity of alternate allele/  
440 (alternate intensity + wild-type intensity), following the method previously developed and  
441 validated by Hinds, et al.<sup>46</sup>. For validation of this method of detecting somatic mutations, we  
442 evaluated 149 MEGA<sup>EX</sup>-genotyped patients with a putative *JAK2* mutation and performed NGS  
443 analysis on the same DNA sample. The two genotyping methods demonstrated high concordance  
444 down to the NGS limit of detection of 5% VAF ( $R^2=0.9931$ ). Because the MEGA<sup>EX</sup>-sequenced  
445 DNA samples were not available for *DNMT3A*, *TET2*, or *ASXL1* at the time of the present study,  
446 an alternative method was employed for these genes. The mean BAF and its standard deviation  
447 were calculated for the population under 40 years of age. Detectable CHIP is extremely rare before  
448 this age, allowing for the determination of the noise in BAF measurements at baseline. The BAFs  
449 of the over-40 population were normalized to the under-40 mean and standard deviation.  
450 Individuals with a normalized BAF greater than or equal to 6 standard deviations above the mean  
451 were considered to have a somatic CHIP mutation.

#### 452 **mCAs detection**

##### 453 ***UKB***

454 The detection of mCAs from genome-wide array genotyping of blood DNA in the UKB has been  
455 described in detail previously<sup>64,65</sup>. Briefly, among 447,828 genotyped individuals in the UKB who  
456 passed sample quality control criteria, intensities from the genotyping arrays were used to yield  
457  $\log_2R$  ratio and BAF for each SNP, and the Eagle2 software<sup>66</sup> was used to phase SNPs. mCAs  
458 calling was performed by leveraging long-range phase information to search for allelic imbalances

459 between maternal and paternal allelic fractions across contiguous genomic segments.  
460 Constitutional duplications and low-quality calls were filtered out, and cell fraction was estimated  
461 as previously described<sup>65</sup>.

462

### 463 ***MGBB***

464 The detection of mCAs in the MGBB was previously described<sup>33</sup>. Briefly, among 22,143  
465 participants who had available probe raw intensity data (IDAT) files for mCAs calling, genotype  
466 clustering was performed using the Illumina GenCall algorithm, and the resulting GTC genotype  
467 files were converted to VCF files using the bcftools gtc2vcf plugin  
468 (<https://github.com/freeseek/gtc2vcf>). Genotype phasing was performed using SHAPEIT<sup>467</sup>, and  
469 the phased genotypes were ligated across overlapping windows using bcftools concat  
470 (<https://github.com/samtools/bcftools>). mCAs detection in the MGBB was performed using  
471 MoChA (<https://github.com/freeseek/mocha>), a workflow to process raw genotypes and probe  
472 intensities to the final mCAs callset. Poor quality sample, defined as having a call rate below 0.97,  
473 BAF auto-correlation across heterozygous sites greater than 0.03, likely germline calls, or runs of  
474 homozygosity identified according to standard filtering practices described in the MoChA online  
475 documentation, were excluded from further analysis.

476

### 477 ***Vanderbilt BioVU***

478 A total of 51,028 participants in the Vanderbilt BioVU had their blood DNA genotyped on the  
479 Illumina Multi-Ethnic Genotyping Array-Expanded (MEGA<sup>EX</sup>). mCAs detection in BioVU was  
480 then performed using MoChA (<https://github.com/freeseek/mocha>). Samples that did not pass  
481 quality control criteria were excluded from the analysis.

482

### 483 ***Millions Veteran Program***

484 DNA extracted from the whole blood of 613,329 participants in the Millions Veteran Program  
485 (MVP) was genotyped using a customized Affymetrix Axiom Biobank array, the MVP 1.0  
486 Genotyping Array, followed by standard QC and imputation as described elsewhere<sup>68</sup>. mCAs were  
487 detected using the MoChA pipeline (<https://github.com/freeseek/mocha>). Samples that did not  
488 pass quality control criteria were excluded.

489

### 490 **GWAS and Meta-analysis**

491 GWAS for overall CHIP, *DNMT3A*, and *TET2* CHIP was performed using REGENIE<sup>69</sup> (in UKB,  
492 MGB, and BioVU cohort) or SAIGE<sup>70</sup> (in TOPMed cohort, previously reported in Bick et al.<sup>22</sup>).  
493 We performed GWAS in UKB, MGBB, and BioVU cohorts separately with CHIP status (VAF $\geq$ 2%)

494 as "1", "0" otherwise) as the outcome, fitting a logistic mixed model, adjusting for age at enrolment,  
495 age<sup>2</sup>, sex, first ten principal components, self-reported ethnicity, and genotyping batch (where  
496 appropriate). Here, only unrelated samples (one sample from each pair of 1<sup>st</sup> or 2<sup>nd</sup>-degree related  
497 samples, or  $\geq 3$ -degree relatedness) with genotype missingness  $< 10\%$  and non-missing  
498 outcome/covariates were included in the analysis. GWAS was performed in two steps: 1) prepare  
499 the null model using high-quality SNP in a leave-one-out cross-validation approach (REGENIE "-  
500 -loocv" flag), and 2) perform the single variant association. In Step 1, we used  $\sim 500$ k directly  
501 genotyped SNP after excluding variants with minor allele frequency (MAF) below 5%, genotype  
502 missingness above 10%, and Hardy-Weinberg equilibrium  $P > 1 \times 10^{-15}$ . In Step 2, we used imputed  
503 GWAS variants with a minor allele count  $\geq 20$  for the association test. To account for the case-  
504 control imbalance, we used the REGENIE "--firth" flag at GWAS  $P < 0.01$  to implement the Firth  
505 likelihood test to control Type 1 errors.

506 Next, we meta-analyzed GWAS results from the four cohorts using inverse-variance  
507 weighted fixed-effect meta-analysis and Cochran's  $Q$ -test for heterogeneity in GWAMA  
508 software<sup>71</sup>. Here, variants at  $MAF \geq 0.1\%$  and present in  $\geq 2$  studies were included in the meta-  
509 analysis. Finally, variants were considered genome-wide significant at  $P \leq 1.67 \times 10^{-8}$ , considering  
510 1-million independent SNP and three outcomes tested at a 5% significance level (i.e.,  $5 \times 10^{-8}/3$ ).

511

## 512 **Conditional and Joint Analysis (COJO)**

513 Conditional and joint (COJO)<sup>72,73</sup> analyses of summary statistics from multi-ancestry meta-  
514 analyses of CHIP, *DNMT3A*, and *TET2* CHIP GWAS were performed using a multi-ancestry LD  
515 reference prepared from the UKB imputed GWAS dataset that included all the 191k unrelated  
516 samples used in our UKB CHIP GWAS. The LD panel included variants with  $MAF \geq 0.1\%$  and  
517  $INFO \geq 0.3$ . In the COJO analyses, we conditioned the lead variant (false discovery rate (FDR)  
518  $< 5\%$ ) from each chromosome, and independent variants (FDR  $< 5\%$  and LD with the conditioned  
519 variant  $< 0.8$ ) were included iteratively. Finally, all variants were fitted simultaneously in the joint  
520 analyses when multiple independent variants were detected in the same chromosome. Independent  
521 variants at  $P \leq 1.67 \times 10^{-8}$  were considered genome-wide significant.

## 522 **SNP-based heritability ( $h^2_{SNP}$ )**

523 We estimated  $h^2_{SNP}$  using the summary statistics from the multi-ancestry meta-analysis of CHIP  
524 GWAS. We used the SumHer function of LDAK software<sup>74,75</sup> with precomputed LD tagging  
525 (BLD-LDAK model: <https://genetics.ghpc.au.dk/doug/bld.ldak.genotyped.gbr.tagging.gz>)  
526 prepared from directly genotyped UKB EUR sample. The BLD-LDAK EUR LD tagging was  
527 prepared using 577,457 non-ambiguous directly genotyped SNP from 2,000 white British  
528 individuals. Using 573,701 overlapping SNP from the summary statistics,  $h^2_{SNP}$  was estimated on  
529 a liability scale assuming a sample and population CHIP prevalence of 5%.

## 530 **MashR**

531 To nominate potentially associated variants, we leveraged the observation that myeloproliferative  
532 neoplasm (MPN) shared strong germline genetic susceptibility with CHIP<sup>30</sup>. We used MPN  
533 GWAS summary statistics from Bao, et al.<sup>30</sup>, and applied mashR (Multivariate Adaptive  
534 Shrinkage in R)<sup>34</sup> to 6,749,139 variants across MPN, CHIP, *DNMT3A*, and *TET2* using the  
535 exchangeable *Z* statistic model. Briefly, we fit the empirical Bayes prior by using the maximum  
536 SNP across each of the 1,703 linkage disequilibrium (LD) blocks specified in Pickrell, et al.<sup>76</sup> and  
537 used a random sampling of 40,000 SNPs to estimate the relative abundance of each pattern in the  
538 overall data set. Armed with this prior information, we then estimated the likelihood and computed  
539 posteriors on all variants.

540

## 541 **Statistical fine-mapping**

542 To infer putative causal variants in the associated loci, we conducted LD-informed statistical fine-  
543 mapping. We derived the LD-matrix of tested variants in each locus using UK Biobank imputed  
544 dosage of European ancestries by LDstore2 software (version 2.0)<sup>77</sup>. Using derived LD-matrices,  
545 we applied statistical fine-mapping using the summary statistics obtained from the European meta-  
546 analysis (only included GWAS of EUR samples from UKB, TOPMed, MGGB, BioVU) by  
547 FINEMAP software (version 1.4)<sup>24</sup>. To obtain consistent statistical power for each variant, we  
548 only kept variants tested in at least 200,000 individuals.

549

## 550 **Similarity-based gene polygenic prioritization of causal genes**

551 We implemented PoPS to leverage the full genome-wide signal for nominating causal genes.  
552 Details of these methods have been described elsewhere<sup>25</sup>. Briefly, PoPS is a novel similarity-  
553 based gene prioritization approach that assesses the polygenic enrichments of gene features,  
554 including cell-type-specific gene expression, protein-protein interaction networks, and biological  
555 pathways, through training linear models to predict gene-level association scores from those  
556 features and converting the gene p-values from the linear models to *Z*-scores that reflect the  
557 confidence on its causal role to the given locus. We used the summary statistics of UKB CHIP,  
558 *DNMT3A*, and *TET2* GWAS and the same LD reference panel of 191k UKB samples used in  
559 COJO analysis. In total, 57,543 features were considered for analysis, and those who passed  
560 marginal feature selection were carried forward to the linear models for computation. We  
561 computed a PoPS score for all protein-coding genes within a defined 500kb window around each  
562 of the significant genomic regions and prioritized the gene with the highest PoPS score in each  
563 locus.

564



## 565 Mendelian randomization

566 All procedures for the MR analysis between CHIP and CAD were consistent with current  
567 recommendations for MR studies<sup>78</sup>. IVs detected in European-only CHIP GWAS were used for  
568 this causal analysis. While genetic predispositions for CHIP overlap with those for LTL, previous  
569 MR studies support inverse causality for LTL on CAD<sup>79</sup>, implying complex causal relationships  
570 between CHIP, LTL, and CAD<sup>23</sup>. Thus, we carefully selected instrumental variables (IVs) to avoid  
571 clear violations of MR assumptions by excluding IVs 1) associated with known confounders  
572 between CHIP and CAD, including hypercholesterolemia, hypertension, type 2 diabetes, body  
573 mass index, smoking status, or 2) having more robust associations with LTL than with CAD, and  
574 3) having inverse effect sizes for LTL and CAD, accounting for the inverse causal association  
575 between LTL and CAD. We used CAD GWAS summary statistics from  
576 CARDIOGRAMplusC4D<sup>80</sup> for the outcome (last accessed March 2022; downloaded from:  
577 <http://www.cardiogramplusc4d.org/>). We downloaded summary statistics from OpenGWAS  
578 project<sup>81,82</sup> for excluding IVs which strongly ( $P < 5 \times 10^{-8}$ ) associated with known confounders  
579 between CHIP and CAD, including hypercholesterolemia (ukb-b-12651), hypertension (ukb-d-  
580 I9\_HYPTENS), type 2 diabetes (ebi-a-GCST007518), body mass index (ukb-b-2303), smoking  
581 status (ukb-b-20261). We used the full summary statistics for LTL GWAS from the previous study  
582 in UKB to inspect the association with LTL<sup>79</sup>. Since we do not have many SNPs that pass through  
583 the genome-wide significance, particularly for *TET2*, we used the multi-ancestry meta-analysis of  
584 *DNMT3A* and *TET2* CHIP summary statistics and MR using the robust adjusted profile score (MR-  
585 RAPS), which allows for the inclusion of weak IVs<sup>42</sup>, as the primary method. We performed  
586 sensitivity analyses using inverse-variance weighted (IVW)<sup>83</sup>, weighted median<sup>83</sup>, weighted  
587 mode<sup>84</sup>, MR-Egger<sup>85</sup>, and MR-PRESSO<sup>86</sup> methods available in the TwoSampleMR<sup>82</sup> package in  
588 R. For all MR methods except for MR-RAPS, genome-wide significance ( $P < 5 \times 10^{-8}$ ) was  
589 considered as the criteria for the IV assumption of robust relevance (the first assumption of MR).  
590 We relaxed this assumption for MR-RAPs to  $P < 1 \times 10^{-3}$ ,  $1 \times 10^{-4}$ , and  $1 \times 10^{-5}$ . IVs were clumped into  
591 independent loci  $< 10$  Mb apart and in the linkage equilibrium ( $R^2 > 0.001$  calculated in European  
592 ancestry in UKB) using PLINK (v1.90b6.24)<sup>87</sup>. Due to the limited availability of CHIP GWAS to  
593 date, we could not use an independent cohort for IV discovery for MR-RAPS and Steiger filtering  
594 to avoid the potential "winner's curse".

595

## 596 PheWAS analysis

597 The PheWAS of CHIP and mCAs with incident phenotypes across all disease organ system  
598 categories were performed using Cox proportional hazards models, adjusting for age, age<sup>2</sup>, sex  
599 (not used for ChrY and ChrX mCAs analysis), smoking status (using a 25-factor smoking status  
600 adjustment in the UKB and current/prior/never smoker status in other cohorts), tobacco use  
601 disorder, and principal components 1-10 of genetic ancestry. The primary comparative analysis  
602 was conducted among individuals from UKB who had both CHIP and mCAs calls available.

603 Additionally, in the secondary analysis, mCAs associations were meta-analyzed across the multi-  
604 ancestry study population of UKB, MGBB, BioVU, and MVP. Time since DNA collection was  
605 used as the underlying timescale. The proportional hazards assumption was assessed using  
606 Schoenfeld residuals and was not rejected. Individuals with a history of hematological cancer  
607 before DNA collection were excluded. To address multiple testing, an association between CHIP  
608 or mCAs and incident health outcomes with  $FDR < 0.05$  was considered significant. Analyses of  
609 incident events were performed separately in each biobank using the survival package in R (version  
610 3.5, R Foundation). Meta-analyses of the mCAs results were performed using a fixed-effects  
611 model from the "meta" R package.

612

### 613 **CHIP associations at the cell-type level**

614 scDRS group analysis was used to assess the polygenic associations of CHIP, *DNMT3A*, and *TET2*  
615 at cell type and tissue level. Details of the methods have been described elsewhere<sup>31</sup>. Briefly,  
616 scDRS is a novel statistical method that associates individual cells in a scRNA-seq data to a trait  
617 GWAS based on the aggregate expression across a set of putative GWAS trait genes, assessing  
618 statistical significance using appropriately matched control genes; furthermore, the scDRS group  
619 analysis computes a p-value for a cell group (e.g., cell type or tissue) based on the association of  
620 cells within the given cell group. Following the scDRS guideline, the putative trait gene sets were  
621 constructed as the top 1,000 MAGMA genes, where MAGMA<sup>88</sup>, an existing gene-scoring method,  
622 was applied to GWASs from UKB participants of European ancestry using a set of 489 unrelated  
623 individuals of European ancestry from phase 3 1000 Genomes Project as an LD reference panel<sup>89</sup>.  
624 Two scRNA-seq data sets were used for this analysis: TMS mouse cell atlas<sup>44</sup> (FACS data with  
625 110,824 cells, 23 tissues, and 103 cell types with more than 50 cells) and TS human cell atlas<sup>45</sup>  
626 (FACS data with 26,813 cells, 24 tissues, and 68 cell types with more than 50 cells). Multiple  
627 testing correlation (FDR) was applied to each trait separately across all cell types (103 for TMS  
628 and 68 for TS) or across all tissues (23 for TMS and 24 for TS). To increase power, associations  
629 were considered significant at  $FDR < 0.3$ , and all suggestive associations with  $P < 0.01$  were reported.  
630 Sensitivity analyses were conducted by repeating the analysis using downsampled scRNA-seq data  
631 (to 50K cells) and downsampled putative trait gene sets (to 500 genes) separately, each with 20  
632 repetitions.

633

## 634 **Data availability**

635 All univariable summary statistics for genotype association with CHIP will be available at the time  
636 of publication. Epigenome annotation tracks: We obtained chromHMM100 tracks from diverse  
637 primary human cells from the NIH Epigenome Roadmap ([http://dcc.blueprint-epigenome.eu/#/md/secondary\\_analysis/Segmentation\\_of\\_ChIP-Seq\\_data\\_20140811](http://dcc.blueprint-epigenome.eu/#/md/secondary_analysis/Segmentation_of_ChIP-Seq_data_20140811)), and  
638 additional immune-specific human primary and cell lines from the Blueprint consortium,  
639 [https://egg2.wustl.edu/roadmap/data/byFileType/chromhmmSegmentations/ChmmModels/core](https://egg2.wustl.edu/roadmap/data/byFileType/chromhmmSegmentations/ChmmModels/coreMarks/jointModel/final)  
640 [Marks/jointModel/final](https://egg2.wustl.edu/roadmap/data/byFileType/chromhmmSegmentations/ChmmModels/coreMarks/jointModel/final). Whole-blood eQTL summary statistics: Summary statistics from whole-  
641 blood cis-eQTL analysis from 31,683 individuals were downloaded from <https://eqtlgen.org>. Code  
642 used to generate all data in main and supplemental tables and figures will be provided in a publicly  
643 accessible archive at the time of publication.

## 645 **Acknowledgments**

646 We thank the investigators and their studies for contributing samples and/or data to the current  
647 work and the participants in those studies who made this research possible. This research has been  
648 conducted using the UK Biobank Resource under Application Number 7089 and 50834. This  
649 research is based on data from the Vanderbilt BioVU, which is supported by NIH Grant UL1  
650 RR024975-01 and UL1 TR000445-06. This research is also based on data from the Million Veteran  
651 Program, Office of Research and Development, Veterans Health Administration, and was  
652 supported by Million Veteran Program-MVP000. This publication does not represent the views of  
653 the Department of Veteran Affairs or the United States Government.

## 654 **Fundings**

655 Z.Y. is supported by a grant from NHLBI (5T32HL007604-37). A.G.B. is supported by a Burroughs  
656 Wellcome Foundation Career Award for Medical Scientists and the NIH Director's Early Independence  
657 Award (DP5-OD029586). A.J.S. is supported by NIH grant F30-DK127699. A.J.S., M.A.R., and H.A.K.  
658 are supported by NIH grant T32-GM007347. A.N. is supported by Knut and Alice Wallenberg Foundation  
659 (KAW 2017.0436). A.P.R. is supported by NIH grants R01 HL148565 and R01 HL146500. B.L.E. is  
660 supported by Leducq Foundation. G.G. is supported by NIH grants R01 MH104964 and R01 MH123451,  
661 and Stanley Center for Psychiatric Research. K.C., Y.V.S., and P.W.F.W are supported by Million Veteran  
662 Program (MVP) grant numbers I01-BX003340 and I01-BX004821. K.P. is supported by grants from the  
663 NHLBI (5-T32HL007208-43). M.C.H. is supported by the American Heart Association (940166 and  
664 979465). P.N. is supported by grants from the NHLBI (R01HL142711, R01HL127564, R01HL148050,  
665 R01HL151283, R01HL148565, R01HL135242, R01HL151152), National Institute of Diabetes and  
666 Digestive and Kidney Diseases (R01DK125782), Fondation Leducq (TNE-18CVD04), and Massachusetts  
667 General Hospital (Paul and Phyllis Fireman Endowed Chair in Vascular Medicine). P.T.E. is supported by  
668 the National Institutes of Health (1R01HL092577), the American Heart Association Strategically Focused  
669 Research Networks (18SFRN34110082), and the European Union (MAESTRIA 965286). S.J. is supported  
670 by the Burroughs Wellcome Fund Career Award for Medical Scientists, Fondation Leducq (TNE-  
671 18CVD04), the Ludwig Center for Cancer Stem Cell Research at Stanford University, and the National

672 Institutes of Health (DP2-HL157540). T.M.M. is supported by NIH grant T32-HL144446. V.G.S. is  
673 supported by NIH grants R01 DK103794 and R01 HL146500.

674

## 675 **Author Contributions**

676 A.G.B. and P.N. designed and conceived the study. A.G.B. and P.N. supervised the study. M.M.U.,  
677 Z.Y., J.S.W., T.N., A.N., S.M.U., S.K., S.M.Z., K.P., A.J.S., T.M.M., M.Y.W., S.M.H., R.B.,  
678 S.D.J., M.R., M.C.H., W.E.H., M.J.Z., V.G.S., G.K.G., C.J.G., H.A.K., P.T.E., K.C., Y.S., P.W.,  
679 S.P., G.G., Y.X., M.R.S., A.P.R., S.J., B.L.E., A.G.B., and P.N. acquired, analyzed or interpreted  
680 the data. M.M.U., Z.Y., T.N., S.M.U., S.K., S.M.Z., A.B., and P.N. drafted the manuscript. All  
681 authors critically reviewed the manuscript.

682

## 683 **Competing Interests**

684 All unrelated to the present work: A.G.B. is a scientific co-founder and has equity in TenSixteen  
685 Bio. B.L.E. has received research funding from Celgene, Deerfield, Novartis, and Calico and  
686 consulting fees from GRAIL. B.L.E. is a member of the scientific advisory board and shareholder  
687 for Neomorph Therapeutics, TenSixteen Bio, Skyhawk Therapeutics, and Exo Therapeutics.  
688 M.C.H. has received consulting fees from CRISPR Therapeutics and is on the medical advisory  
689 board of Miga Health. P.N. reports grant support from Amgen, Apple, AstraZeneca, Novartis, and  
690 Boston Scientific, consulting income from Apple, AstraZeneca, Blackstone Life Sciences,  
691 Genentech, and Novartis, and spousal employment at Vertex, all unrelated to the present work.  
692 P.N., A.G.B., S.J., and B.E. are scientific advisors with equity in TenSixteen Bio, which had no  
693 role in the present work. P.T.E. receives sponsored research support from Bayer AG and IBM  
694 Research; he has also served on advisory boards or consulted for Bayer AG, MyoKardia, and  
695 Novartis. S.J. is a consultant to Novartis, Roche Genentech, AVRO Bio, and Foresite Labs, and  
696 on the scientific advisory board for Bitterroot Bio, founder and equity holder of TenSixteen Bio.  
697 V.G.S. serves as an advisor to and/or has equity in Branch Biosciences, Ensoma, Novartis, Forma,  
698 Sana Biotechnology, and Cellarity. All other authors declare that they have no competing interests.

699

## 700 References

701

- 702 1. Xie, M. *et al.* Age-related mutations associated with clonal hematopoietic expansion and  
703 malignancies. *Nat Med* **20**, 1472-8 (2014).
- 704 2. Genovese, G. *et al.* Clonal hematopoiesis and blood-cancer risk inferred from blood DNA  
705 sequence. *N Engl J Med* **371**, 2477-87 (2014).
- 706 3. Jaiswal, S. *et al.* Age-related clonal hematopoiesis associated with adverse outcomes. *N Engl J*  
707 *Med* **371**, 2488-98 (2014).
- 708 4. Delhommeau, F. *et al.* Mutation in TET2 in myeloid cancers. *N Engl J Med* **360**, 2289-301  
709 (2009).
- 710 5. Ley, T.J. *et al.* DNMT3A mutations in acute myeloid leukemia. *N Engl J Med* **363**, 2424-33  
711 (2010).
- 712 6. Je, E.M., Yoo, N.J., Kim, Y.J., Kim, M.S. & Lee, S.H. Mutational analysis of splicing machinery  
713 genes SF3B1, U2AF1 and SRSF2 in myelodysplasia and other common tumors. *Int J Cancer*  
714 **133**, 260-5 (2013).
- 715 7. Abdel-Wahab, O. *et al.* ASXL1 mutations promote myeloid transformation through loss of  
716 PRC2-mediated gene repression. *Cancer Cell* **22**, 180-93 (2012).
- 717 8. Coombs, C.C. *et al.* Therapy-Related Clonal Hematopoiesis in Patients with Non-hematologic  
718 Cancers Is Common and Associated with Adverse Clinical Outcomes. *Cell Stem Cell* **21**, 374-382  
719 e4 (2017).
- 720 9. Xia, J. *et al.* Somatic mutations and clonal hematopoiesis in congenital neutropenia. *Blood* **131**,  
721 408-416 (2018).
- 722 10. Hsu, J.I. *et al.* PPM1D Mutations Drive Clonal Hematopoiesis in Response to Cytotoxic  
723 Chemotherapy. *Cell Stem Cell* **23**, 700-713 e6 (2018).
- 724 11. Steensma, D.P. *et al.* Clonal hematopoiesis of indeterminate potential and its distinction from  
725 myelodysplastic syndromes. *Blood* **126**, 9-16 (2015).
- 726 12. Abelson, S. *et al.* Prediction of acute myeloid leukaemia risk in healthy individuals. *Nature* **559**,  
727 400-404 (2018).
- 728 13. Desai, P. *et al.* Somatic mutations precede acute myeloid leukemia years before diagnosis. *Nat*  
729 *Med* **24**, 1015-1023 (2018).
- 730 14. Jaiswal, S. *et al.* Clonal Hematopoiesis and Risk of Atherosclerotic Cardiovascular Disease. *N*  
731 *Engl J Med* **377**, 111-121 (2017).
- 732 15. Bick, A.G. *et al.* Genetic Interleukin 6 Signaling Deficiency Attenuates Cardiovascular Risk in  
733 Clonal Hematopoiesis. *Circulation* **141**, 124-131 (2020).
- 734 16. Bhattacharya, R. *et al.* Clonal Hematopoiesis Is Associated With Higher Risk of Stroke. *Stroke*  
735 **53**, 788-797 (2022).
- 736 17. Yu, B. *et al.* Association of Clonal Hematopoiesis With Incident Heart Failure. *J Am Coll Cardiol*  
737 **78**, 42-52 (2021).
- 738 18. Miller, P.G. *et al.* Association of clonal hematopoiesis with chronic obstructive pulmonary  
739 disease. *Blood* **139**, 357-368 (2022).
- 740 19. Kim, P.G. *et al.* Dnmt3a-mutated clonal hematopoiesis promotes osteoporosis. *J Exp Med*  
741 **218**(2021).

- 742 20. Wong, W.J. *et al.* Clonal hematopoiesis and risk of chronic liver disease. *medRxiv*,  
743 2022.01.17.22269409 (2022).
- 744 21. Bouzid, H. *et al.* Clonal hematopoiesis is associated with protection from Alzheimer's disease.  
745 *medRxiv*, 2021.12.10.21267552 (2021).
- 746 22. Bick, A.G. *et al.* Inherited causes of clonal haematopoiesis in 97,691 whole genomes. *Nature*  
747 **586**, 763-768 (2020).
- 748 23. Nakao, T. *et al.* Mendelian randomization supports bidirectional causality between telomere  
749 length and clonal hematopoiesis of indeterminate potential. *Sci Adv* **8**, eabl6579 (2022).
- 750 24. Benner, C. *et al.* FINEMAP: efficient variable selection using summary data from genome-wide  
751 association studies. *Bioinformatics* **32**, 1493-501 (2016).
- 752 25. Weeks, E.M. *et al.* Leveraging polygenic enrichments of gene features to predict genes  
753 underlying complex traits and diseases. *medRxiv*, 2020.09.08.20190561 (2020).
- 754 26. Ciccia, A. & Elledge, S.J. The DNA damage response: making it safe to play with knives. *Mol*  
755 *Cell* **40**, 179-204 (2010).
- 756 27. Huang, R.X. & Zhou, P.K. DNA damage response signaling pathways and targets for  
757 radiotherapy sensitization in cancer. *Signal Transduct Target Ther* **5**, 60 (2020).
- 758 28. Mencia-Trinchant, N. *et al.* Clonal Hematopoiesis Before, During, and After Human Spaceflight.  
759 *Cell Rep* **33**, 108458 (2020).
- 760 29. Jasra, S. *et al.* High burden of clonal hematopoiesis in first responders exposed to the World  
761 Trade Center disaster. *Nat Med* **28**, 468-471 (2022).
- 762 30. Bao, E.L. *et al.* Inherited myeloproliferative neoplasm risk affects haematopoietic stem cells.  
763 *Nature* **586**, 769-775 (2020).
- 764 31. Zhang, M.J. *et al.* Polygenic enrichment distinguishes disease associations of individual cells in  
765 single-cell RNA-seq data. *bioRxiv*, 2021.09.24.461597 (2021).
- 766 32. Codd, V. *et al.* Polygenic basis and biomedical consequences of telomere length variation. *Nat*  
767 *Genet* **53**, 1425-1433 (2021).
- 768 33. Zekavat, S.M. *et al.* Hematopoietic mosaic chromosomal alterations increase the risk for diverse  
769 types of infection. *Nat Med* **27**, 1012-1024 (2021).
- 770 34. Urbut, S.M., Wang, G., Carbonetto, P. & Stephens, M. Flexible statistical methods for estimating  
771 and testing effects in genomic studies with multiple conditions. *Nat Genet* **51**, 187-195 (2019).
- 772 35. Helgason, H. *et al.* Loss-of-function variants in ATM confer risk of gastric cancer. *Nat Genet* **47**,  
773 906-10 (2015).
- 774 36. Karantanos, T. *et al.* ATM Germline Variant Increases the Risk of MPN Progression. *Blood* **134**,  
775 835-835 (2019).
- 776 37. Li, X. *et al.* High PARP-1 expression predicts poor survival in acute myeloid leukemia and  
777 PARP-1 inhibitor and SAHA-bendamustine hybrid inhibitor combination treatment  
778 synergistically enhances anti-tumor effects. *EBioMedicine* **38**, 47-56 (2018).
- 779 38. Min, J.L. *et al.* Genomic and phenotypic insights from an atlas of genetic effects on DNA  
780 methylation. *Nat Genet* **53**, 1311-1321 (2021).
- 781 39. Weinstock, J.S. *et al.* Clonal hematopoiesis is driven by aberrant activation of TCL1A. *bioRxiv*,  
782 2021.12.10.471810 (2021).
- 783 40. Fuster, J.J. *et al.* Clonal hematopoiesis associated with TET2 deficiency accelerates  
784 atherosclerosis development in mice. *Science* **355**, 842-847 (2017).

- 785 41. Wang, Y. *et al.* Tet2-mediated clonal hematopoiesis in nonconditioned mice accelerates age-  
786 associated cardiac dysfunction. *JCI Insight* **5**(2020).
- 787 42. Zhao, Q., Wang, J., Hemani, G., Bowden, J. & Small, D.S. Statistical inference in two-sample  
788 summary-data Mendelian randomization using robust adjusted profile score. *The Annals of*  
789 *Statistics* **48**, 1742-1769, 28 (2020).
- 790 43. Niroula, A. *et al.* Distinction of lymphoid and myeloid clonal hematopoiesis. *Nat Med* **27**, 1921-  
791 1927 (2021).
- 792 44. Tabula Muris, C. A single-cell transcriptomic atlas characterizes ageing tissues in the mouse.  
793 *Nature* **583**, 590-595 (2020).
- 794 45. Consortium, T.T.S. & Quake, S.R. The Tabula Sapiens: a multiple organ single cell  
795 transcriptomic atlas of humans. *bioRxiv*, 2021.07.19.452956 (2021).
- 796 46. Hinds, D.A. *et al.* Germ line variants predispose to both JAK2 V617F clonal hematopoiesis and  
797 myeloproliferative neoplasms. *Blood* **128**, 1121-8 (2016).
- 798 47. Shiloh, Y. & Ziv, Y. The ATM protein kinase: regulating the cellular response to genotoxic  
799 stress, and more. *Nat Rev Mol Cell Biol* **14**, 197-210 (2013).
- 800 48. Krishnakumar, R. & Kraus, W.L. The PARP side of the nucleus: molecular actions, physiological  
801 outcomes, and clinical targets. *Mol Cell* **39**, 8-24 (2010).
- 802 49. Virgilio, L. *et al.* Identification of the TCL1 gene involved in T-cell malignancies. *Proc Natl*  
803 *Acad Sci U S A* **91**, 12530-4 (1994).
- 804 50. Said, J.W. *et al.* TCL1 oncogene expression in B cell subsets from lymphoid hyperplasia and  
805 distinct classes of B cell lymphoma. *Lab Invest* **81**, 555-64 (2001).
- 806 51. Pekarsky, Y. *et al.* Tcl1 enhances Akt kinase activity and mediates its nuclear translocation. *Proc*  
807 *Natl Acad Sci U S A* **97**, 3028-33 (2000).
- 808 52. Laine, J., Kunstle, G., Obata, T., Sha, M. & Noguchi, M. The protooncogene TCL1 is an Akt  
809 kinase coactivator. *Mol Cell* **6**, 395-407 (2000).
- 810 53. Bycroft, C. *et al.* The UK Biobank resource with deep phenotyping and genomic data. *Nature*  
811 **562**, 203-209 (2018).
- 812 54. Nachun, D. *et al.* Clonal hematopoiesis associated with epigenetic aging and clinical outcomes.  
813 *Aging Cell* **20**, e13366 (2021).
- 814 55. Karlson, E.W., Boutin, N.T., Hoffnagle, A.G. & Allen, N.L. Building the Partners HealthCare  
815 Biobank at Partners Personalized Medicine: Informed Consent, Return of Research Results,  
816 Recruitment Lessons and Operational Considerations. *J Pers Med* **6**(2016).
- 817 56. Danciu, I. *et al.* Secondary use of clinical data: the Vanderbilt approach. *J Biomed Inform* **52**, 28-  
818 35 (2014).
- 819 57. Roden, D.M. *et al.* Development of a large-scale de-identified DNA biobank to enable  
820 personalized medicine. *Clin Pharmacol Ther* **84**, 362-9 (2008).
- 821 58. Benjamin, D. *et al.* Calling Somatic SNVs and Indels with Mutect2. *bioRxiv*, 861054 (2019).
- 822 59. Karczewski, K.J. *et al.* The mutational constraint spectrum quantified from variation in 141,456  
823 humans. *Nature* **581**, 434-443 (2020).
- 824 60. Wang, K., Li, M. & Hakonarson, H. ANNOVAR: functional annotation of genetic variants from  
825 high-throughput sequencing data. *Nucleic Acids Res* **38**, e164 (2010).
- 826 61. Regier, A.A. *et al.* Functional equivalence of genome sequencing analysis pipelines enables  
827 harmonized variant calling across human genetics projects. *Nat Commun* **9**, 4038 (2018).

- 828 62. Jun, G., Wing, M.K., Abecasis, G.R. & Kang, H.M. An efficient and scalable analysis framework  
829 for variant extraction and refinement from population-scale DNA sequence data. *Genome Res* **25**,  
830 918-25 (2015).
- 831 63. Taliun, D. *et al.* Sequencing of 53,831 diverse genomes from the NHLBI TOPMed Program.  
832 *Nature* **590**, 290-299 (2021).
- 833 64. Loh, P.R., Genovese, G. & McCarroll, S.A. Monogenic and polygenic inheritance become  
834 instruments for clonal selection. *Nature* (2020).
- 835 65. Loh, P.R. *et al.* Insights into clonal haematopoiesis from 8,342 mosaic chromosomal alterations.  
836 *Nature* (2018).
- 837 66. Loh, P.R. *et al.* Reference-based phasing using the Haplotype Reference Consortium panel. *Nat*  
838 *Genet* **48**, 1443-1448 (2016).
- 839 67. Delaneau, O., Zagury, J.F., Robinson, M.R., Marchini, J.L. & Dermitzakis, E.T. Accurate,  
840 scalable and integrative haplotype estimation. *Nat Commun* **10**, 5436 (2019).
- 841 68. Klarin, D. *et al.* Genome-wide association study of peripheral artery disease in the Million  
842 Veteran Program. *Nat Med* **25**, 1274-1279 (2019).
- 843 69. Mbatchou, J. *et al.* Computationally efficient whole-genome regression for quantitative and  
844 binary traits. *Nat Genet* **53**, 1097-1103 (2021).
- 845 70. Zhou, W. *et al.* Efficiently controlling for case-control imbalance and sample relatedness in large-  
846 scale genetic association studies. *Nat Genet* **50**, 1335-1341 (2018).
- 847 71. Magi, R. & Morris, A.P. GWAMA: software for genome-wide association meta-analysis. *BMC*  
848 *Bioinformatics* **11**, 288 (2010).
- 849 72. Yang, J. *et al.* Conditional and joint multiple-SNP analysis of GWAS summary statistics  
850 identifies additional variants influencing complex traits. *Nat Genet* **44**, 369-75, S1-3 (2012).
- 851 73. Yang, J., Lee, S.H., Goddard, M.E. & Visscher, P.M. GCTA: a tool for genome-wide complex  
852 trait analysis. *Am J Hum Genet* **88**, 76-82 (2011).
- 853 74. Speed, D. & Balding, D.J. SumHer better estimates the SNP heritability of complex traits from  
854 summary statistics. *Nat Genet* **51**, 277-284 (2019).
- 855 75. Speed, D., Holmes, J. & Balding, D.J. Evaluating and improving heritability models using  
856 summary statistics. *Nat Genet* **52**, 458-462 (2020).
- 857 76. Pickrell, J.K. *et al.* Detection and interpretation of shared genetic influences on 42 human traits.  
858 *Nat Genet* **48**, 709-17 (2016).
- 859 77. Benner, C. *et al.* Prospects of Fine-Mapping Trait-Associated Genomic Regions by Using  
860 Summary Statistics from Genome-wide Association Studies. *Am J Hum Genet* **101**, 539-551  
861 (2017).
- 862 78. Burgess, S. *et al.* Guidelines for performing Mendelian randomization investigations. *Wellcome*  
863 *Open Res* **4**, 186 (2019).
- 864 79. Codd, V. *et al.* Identification of seven loci affecting mean telomere length and their association  
865 with disease. *Nat Genet* **45**, 422-7, 427e1-2 (2013).
- 866 80. Nikpay, M. *et al.* A comprehensive 1,000 Genomes-based genome-wide association meta-  
867 analysis of coronary artery disease. *Nat Genet* **47**, 1121-1130 (2015).
- 868 81. Elsworth, B. *et al.* The MRC IEU OpenGWAS data infrastructure. *bioRxiv*, 2020.08.10.244293  
869 (2020).
- 870 82. Hemani, G. *et al.* The MR-Base platform supports systematic causal inference across the human  
871 phenome. *Elife* **7**(2018).



- 872 83. Bowden, J., Davey Smith, G., Haycock, P.C. & Burgess, S. Consistent Estimation in Mendelian  
873 Randomization with Some Invalid Instruments Using a Weighted Median Estimator. *Genet*  
874 *Epidemiol* **40**, 304-14 (2016).
- 875 84. Burgess, S., Foley, C.N., Allara, E., Staley, J.R. & Howson, J.M.M. A robust and efficient  
876 method for Mendelian randomization with hundreds of genetic variants. *Nat Commun* **11**, 376  
877 (2020).
- 878 85. Burgess, S. & Thompson, S.G. Interpreting findings from Mendelian randomization using the  
879 MR-Egger method. *Eur J Epidemiol* **32**, 377-389 (2017).
- 880 86. Verbanck, M., Chen, C.Y., Neale, B. & Do, R. Detection of widespread horizontal pleiotropy in  
881 causal relationships inferred from Mendelian randomization between complex traits and diseases.  
882 *Nat Genet* **50**, 693-698 (2018).
- 883 87. Purcell, S. *et al.* PLINK: a tool set for whole-genome association and population-based linkage  
884 analyses. *Am J Hum Genet* **81**, 559-75 (2007).
- 885 88. de Leeuw, C.A., Mooij, J.M., Heskes, T. & Posthuma, D. MAGMA: generalized gene-set  
886 analysis of GWAS data. *PLoS Comput Biol* **11**, e1004219 (2015).
- 887 89. Genomes Project, C. *et al.* A global reference for human genetic variation. *Nature* **526**, 68-74  
888 (2015).
- 889

## Figures

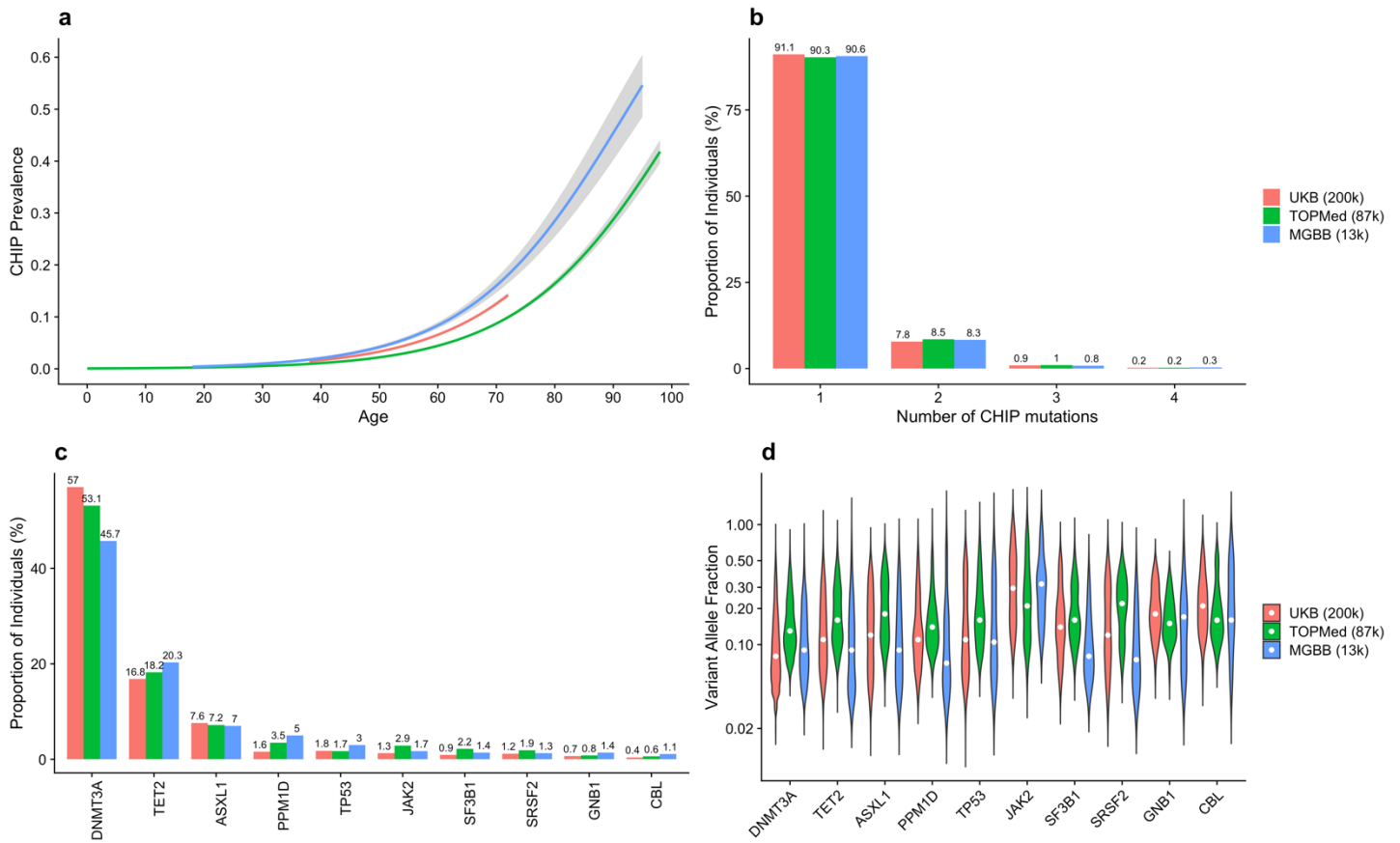


**Fig. 1 | Identifying CHIP in 300,600 whole-genome or whole-exome samples. a**, CHIP prevalence increased with the age of the donor at the time of blood sampling. The centre line represents the general additive model spline, and the shaded region is the 95% confidence interval ( $N_{UKB}=200,128$  WES;  $N_{TOPMed}=87,116$  WGS;  $N_{MGBB}=13,356$  WES). **b**, More than 90% of individuals with CHIP had only one somatic CHIP driver mutation variant identified. **c**, Proportion of individuals carrying a driver mutation in the ten most frequently mutated genes in CHIP. **d**, There was heterogeneity in CHIP clone size as measured by variant allele fraction by CHIP driver gene. Violin plot spanning minimum and maximum values with median variant allele fraction highlighted by white circles. Information on BioVU was not included as CHIP call is array-based. CHIP: clonal hematopoiesis of indeterminate potential; WES: whole-exome samples; WGS: whole-genome samples.

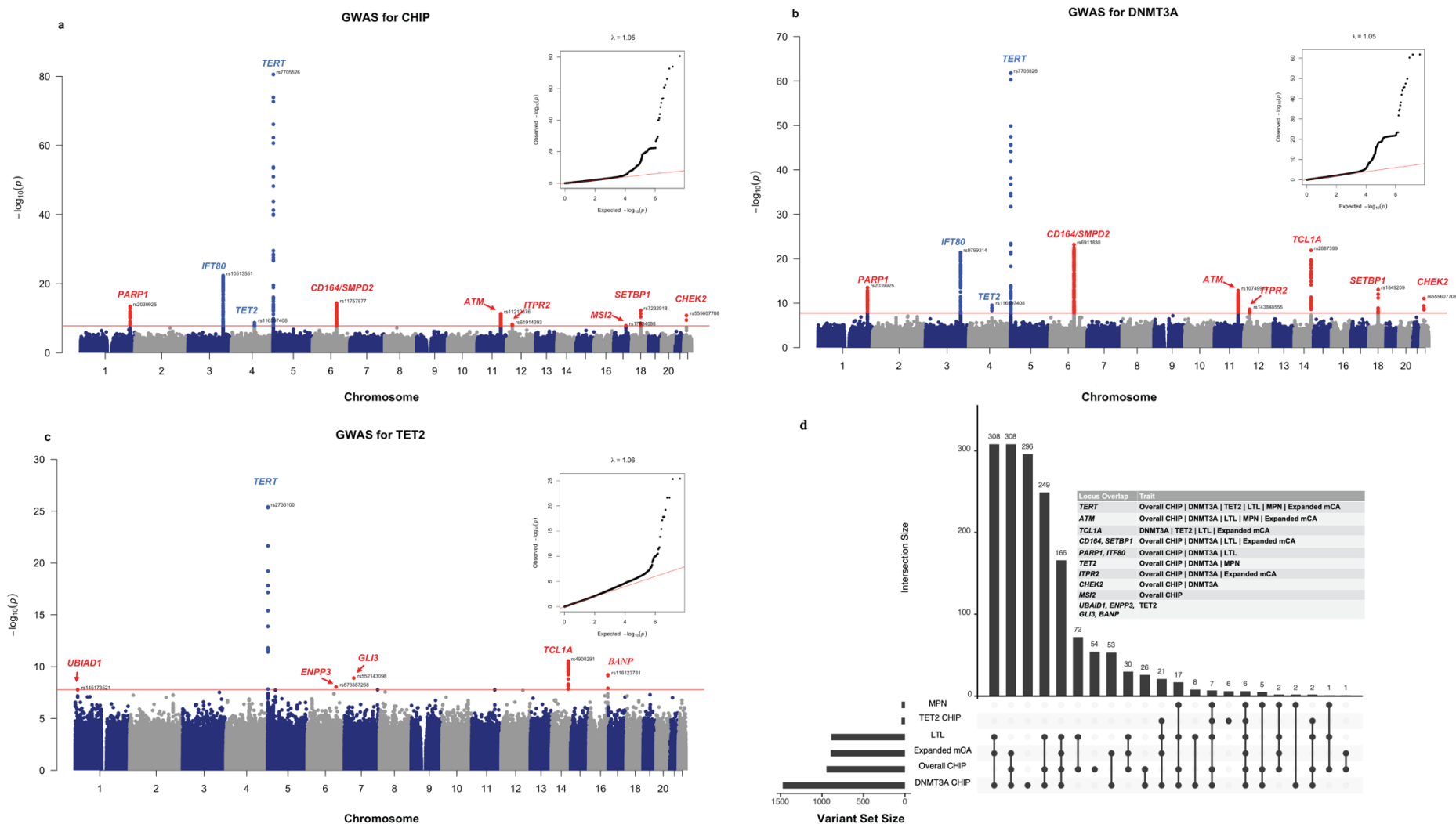


**Fig. 2 | Genetic determinants of CHIP, DNMT3A, and TET2.** Genome-wide meta-analyses of CHIP identified (a) ten genome-wide-significant ( $P < 1.67 \times 10^{-8}$ ) regions for overall CHIP ( $n = 17,044$  cases and  $n = 306,068$  controls), (b) ten for *DNMT3A* CHIP ( $n = 8,949$  cases and  $n = 307,971$  controls), and (c) six for *TET2* CHIP ( $n = 2,851$  cases and  $n = 307,527$  controls). Previously known loci in blue, and new loci in red. **d**, Overlap of significant variants from (a-c) with GWAS of myeloproliferative neoplasm (MPN)<sup>30</sup>, leukocyte telomere length (LTL)<sup>32</sup>, and expanded mosaic chromosomal alterations (mCAs)<sup>33</sup>. Only genome-wide significant ( $P < 5 \times 10^{-8}$ ) variants from MPN, LTL, and expanded mCAs GWAS were considered to compare the overlap with variants from overall CHIP, *DNMT3A*, and *TET2* CHIP GWAS ( $P < 1.67 \times 10^{-8}$ ). CHIP: clonal hematopoiesis of indeterminate potential.

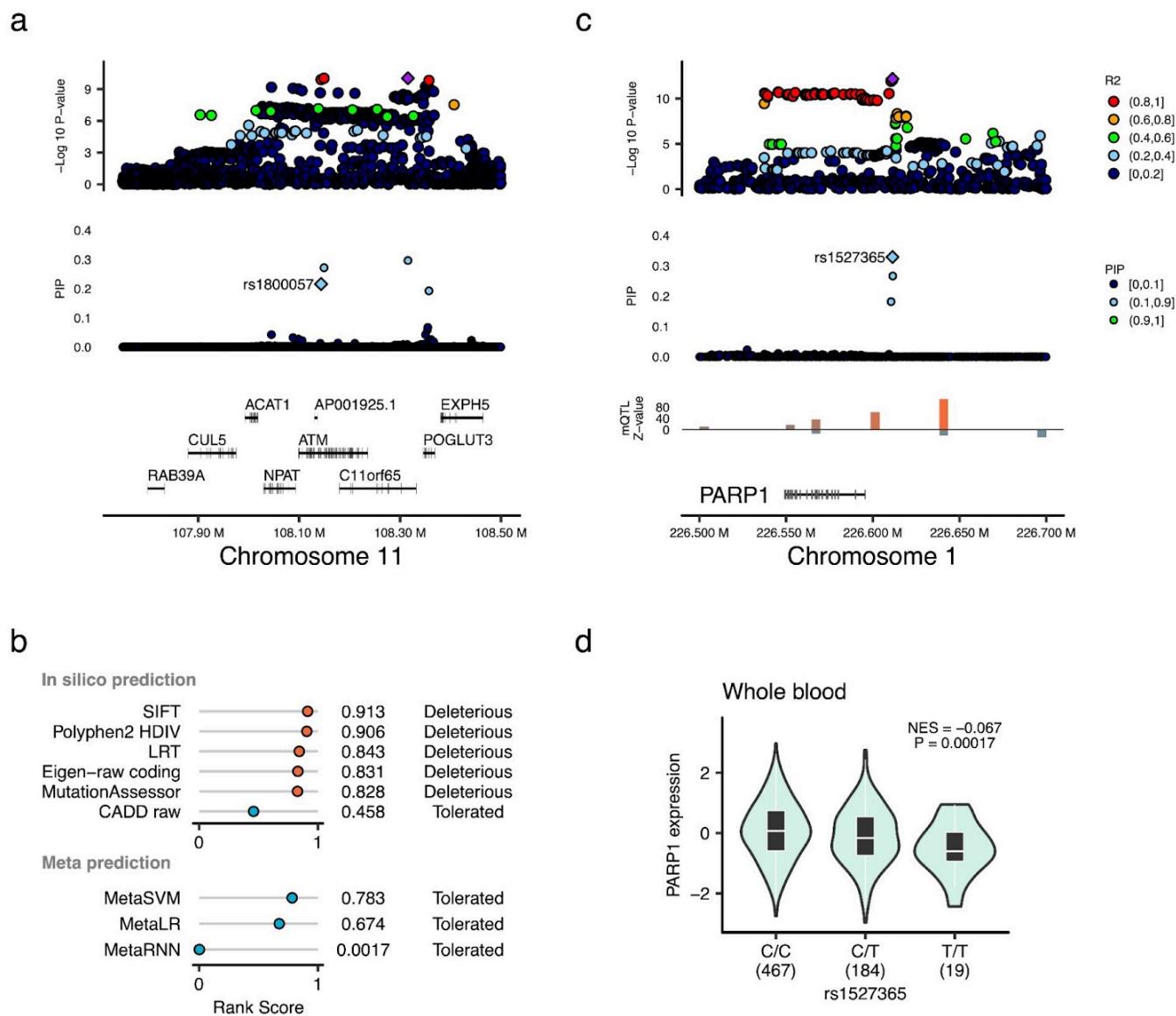


**Fig. 3 | Statistical fine mapping in the genome-wide significant loci. a**, Regional association plot for *ATM* locus. X-axis shows genetic coordinate. Y-axes show  $-\log_{10}$  P-value and PPI. **b**, In-silico functional prediction for putative causal missense variant rs1800057 (ENST00000675843.1:c.3161C>G;p.Pro1054Arg) in *ATM* gene. **c**, Regional association plot for *PARP1* locus. **d**, *PARP1* expression in human whole blood by genotypes at rs1527365 (<https://gtexportal.org/>). The effect allele rs1527365-T is associated with lower expression of *PARP1*. NES: normalized effect size.

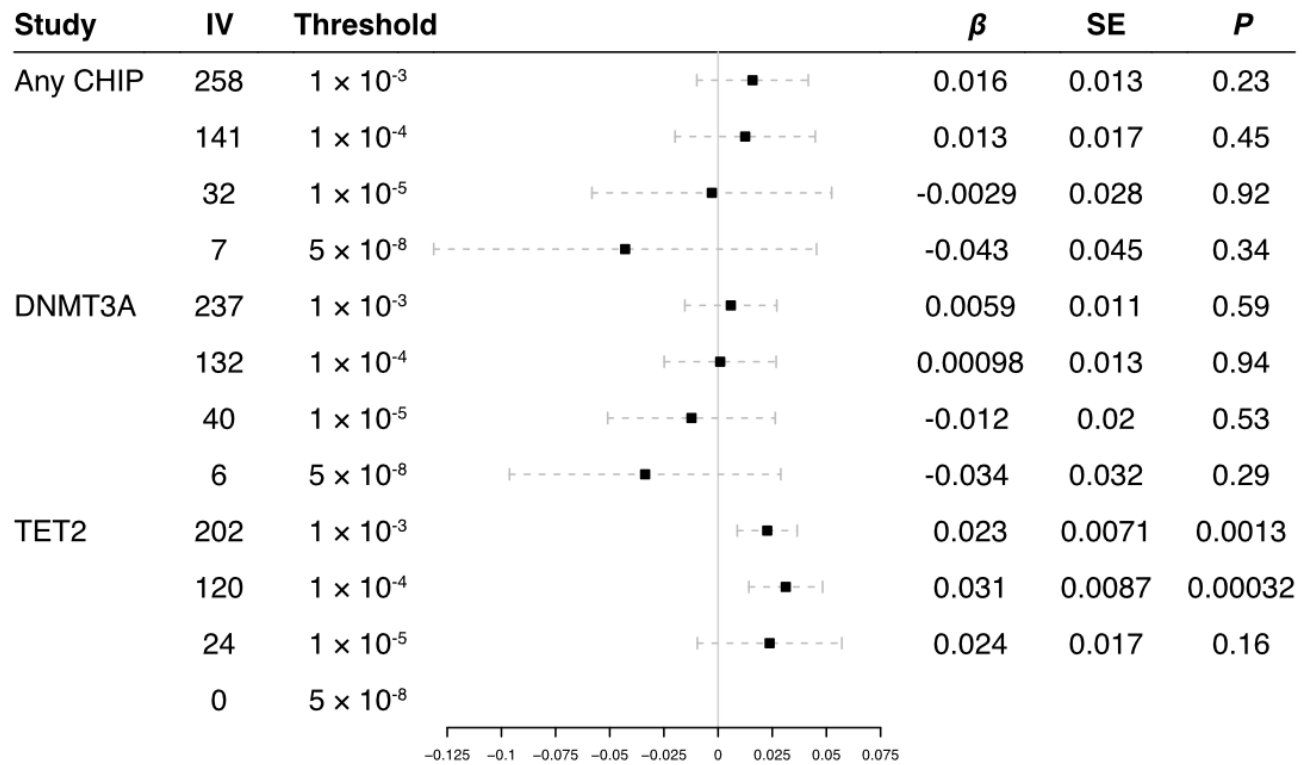


**Figure 4. Mendelian randomization for CHIP and CAD using MR-RAPS.** MR-RAPS for CHIP and CAD including weak IVs. We selected IVs using GWAS summary statistics for any CHIP, *DNMT3A*, and *TET2*, and filtered out the IVs with 1) associated with known confounders between CHIP and CAD, including hypercholesterolemia, hypertension, type 2 diabetes, body mass index, smoking status, or 2) having more robust associations with LTL than with CAD, and 3) having inverse effect sizes for LTL and CAD, accounting for the inverse causal association between LTL and CAD. 1) more robust association with LTL than CAD, and 2) the opposite directionality of the effect for LTL and CAD, to avoid potential confounding by LTL. We used CAD GWAS summary statistics from CARDIOGRAMplusC4D for outcome. CAD: coronary artery disease, CHIP: clonal hematopoiesis of indeterminate potential, IV: instrumental variable, LTL: leukocyte telomere length, SE: standard error.

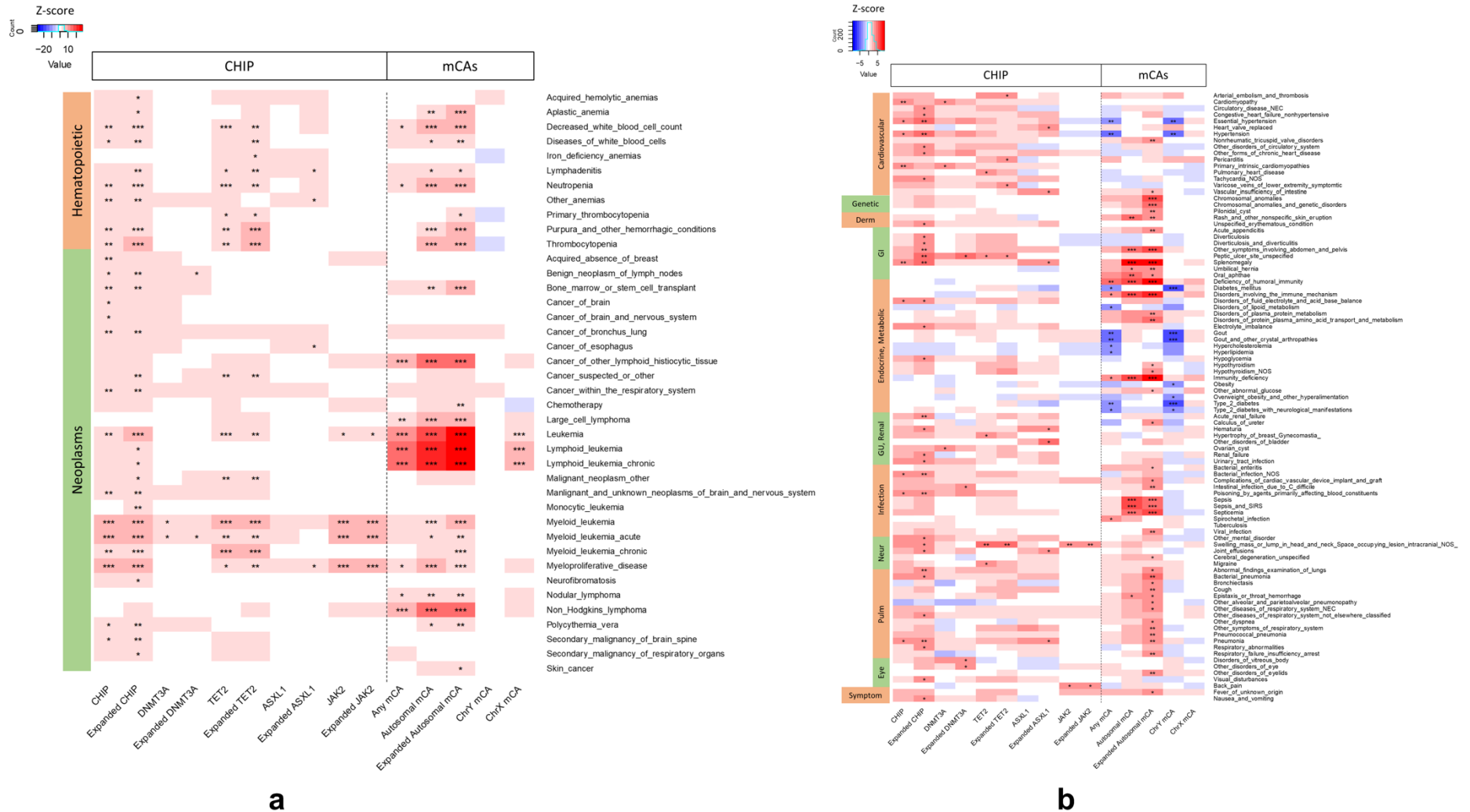


**Figure 5: Heat map of significant associations between CHIP or mCAs and incident conditions from phenome-wide association analysis: (a) Hematopoietic conditions and neoplasms and (b) Non-hematopoietic/neoplastic conditions.** PheCode phenotypes were filtered to those with CHIP or mCA FDR<0.05 among incident phenotypes with at least 5 incident cases. The CHIP and mCA analyses were conducted among the same subset of individuals in the UK Biobank with both CHIP and mCA calls available. All analyses were adjusted for age, age<sup>2</sup>, sex (not used for ChrY and Chr X mCA analysis), smoking status (using a 25-factor smoking status adjustment in the UK Biobank and current/prior/never smoker status in other cohorts), tobacco use disorder, and principal components 1-10 of genetic ancestry. Colors in heat map reflect z-score (beta/se) of associations. \* denotes 0.01≤FDR≤0.05, \*\* denotes 0.0001<FDR≤0.01, \*\*\* denotes FDR<0.0001. CHIP: clonal hematopoiesis of indeterminate potential, mCAs: mosaic chromosomal alterations.

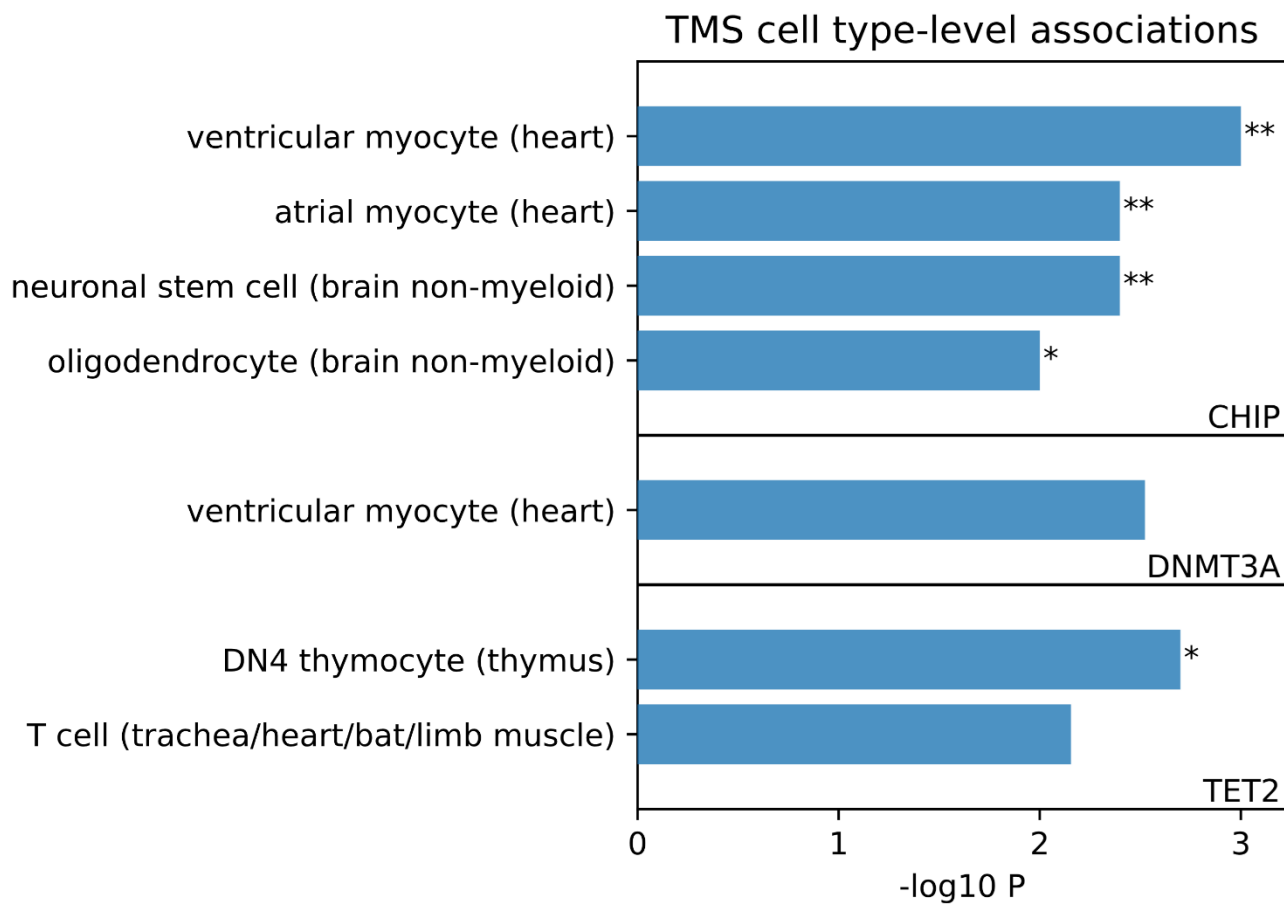


**Figure 6: Cell type-level associations in TMS.** Cell type-level associations in TMS. The x-axis represents scDRS  $-\log_{10}$  cell type-level association p-values while the y-axis represents potentially associated cell types ( $P < 0.01$ ) for the 3 traits, ordered by significance. \* denotes  $FDR < 0.3$ , \*\* denotes  $FDR < 0.2$ , and \*\*\* denotes  $FDR < 0.1$  across all cell types for a given trait. CHIP: clonal hematopoiesis of indeterminate potential. TMS: Tabula Muris Senis.